

University of Nebraska - Lincoln

DigitalCommons@University of Nebraska - Lincoln

Civil Engineering Theses, Dissertations, and
Student Research

Civil Engineering


Summer 7-2-2018

Artificial Neural Network and Finite Element Modeling of Nanoindentation Tests on Silica

KIANOOSH KOOCHEKI

University of Nebraska - Lincoln, koocheki@gmail.com

Follow this and additional works at: <http://digitalcommons.unl.edu/civilengdiss>

 Part of the [Civil and Environmental Engineering Commons](#), and the [Engineering Science and Materials Commons](#)

KOOCHEKI, KIANOOSH, "Artificial Neural Network and Finite Element Modeling of Nanoindentation Tests on Silica" (2018).
Civil Engineering Theses, Dissertations, and Student Research. 124.
<http://digitalcommons.unl.edu/civilengdiss/124>

This Article is brought to you for free and open access by the Civil Engineering at DigitalCommons@University of Nebraska - Lincoln. It has been accepted for inclusion in Civil Engineering Theses, Dissertations, and Student Research by an authorized administrator of DigitalCommons@University of Nebraska - Lincoln.

ARTIFICIAL NEURAL NETWORK AND FINITE ELEMENT
MODELING OF NANOINDENTATION TESTS ON SILICA

by

Kianoosh Koocheki

A THESIS

Presented to the Faculty of
The Graduate College at the University of Nebraska
In Partial Fulfillment of Requirements
For the Degree of Master of Science

Major: Civil Engineering

Under the Supervision of Professor Chung R. Song
Lincoln, Nebraska

June 2018

ARTIFICIAL NEURAL NETWORK AND FINITE ELEMENT
MODELING OF NANOINDENTATION TESTS ON SILICA

Kianoosh Koocheki, M.S.

University of Nebraska, 2018

Advisor: Chung R. Song

Two major forms of Silica include the crystalline form named Quartz which consist of the sand grains in nature, and amorphous form named Silica Glass or Fused Silica which is commonly known as glass. Fused Silica is an amorphous crystal that can show plastic behavior at micro-scale despite its brittle behavior in large scales. Due to the amorphous and ductile nature of Fused Silica, this behavior may not be explained well using the traditional dislocation-based mechanism of plasticity for crystalline solids. The crystal plasticity happens due to shear stress and stored energy in the material as dislocations which does not change the volume. In amorphous Fused Silica however, the permanent deformation is mainly caused by densification of the material under localized loading in addition to plastic flow caused by shear stress. This behavior is particularly true in the case of nanoindentation testing. Due to this densifying behavior, modeling the material using constitutive models such as Drucker-Prager/Cap can be quite helpful to further expand the model parameters to be used for geomaterials.

Nanoindentation tests were performed on Fused Silica and Quartz samples and Finite Element Method (FEM) was used to further investigate the effect of different constitutive model parameters on material behavior. It was observed that, by implementing volumetric hardening in constitutive models, the FEM results were in better agreement with experimental results in case of both Fused Silica and sand grains. In the second part of the study Artificial Neural Network (ANN) models were used to predict nanoindentation test results for different material parameters as well as indenter shape and geometry. ANN models were trained using FEM results and experimental test results and verified using the remainder of the data. Trained models were then used to study of different scenarios that were not analyzed using FEM or experiments.

KEYWORDS: ANN; FEM; Nanoindentation; Silica; Nonlinear Behavior

ACKNOWLEDGMENTS

This work would have not been possible without guidance and help of my dear advisor Dr. Chung R. Song; Therefore, I will always be grateful and in his debt for teaching me how to be a critical thinker, be creative, always work hard, never give up when facing a challenge, and for helping me develop my academic and research skills. Moreover, Dr. Song has always been supportive in all circumstances and I will always be indebted to him for all he has done for me. I would also thank Prof. Yong-Rak Kim, Dr. Jongwan Eun and Dr. Seunghee Kim for their time and effort to assemble the graduate committee. I will never be able to repay the sacrifice that my parents have always made to pave the way for me to pursue my dreams and to endure being thousands of miles away from me, and I will always be thankful to them. I am also grateful to all the friends and colleagues I met during my course of study at University of Nebraska-Lincoln and Prem S. Paul research building, for giving me a sense of belonging to a great community of scholars, and it will not be possible to name them all since it will be more than one page. I am grateful to all staff at UNL Civil Engineering Department and Graduate Studies that helped me will every related work along the way. Last but not least, this thesis would have not been written almost three years before it was due in form of a Doctoral Dissertation, if it was not with the help of U.S. Customs and Border Protection under Trump administration by preventing me from entering the United States to resume my research after visiting my family in my home country. It was during that time that the idea of using Artificial Neural Networks presented itself to me.

Table of Contents

CHAPTER 1 INTRODUCTION	1
1.1 Problem statement	1
1.2 Research objectives and scope	2
1.3 Organization of thesis.....	3
CHAPTER 2 LITERATURE REVIEW	5
2.1 Nanoindentation Experiments	5
2.2 Constitutive Models	7
2.3 Artificial Neural Network (ANN) Models.....	12
2.3.1 ANN for Nonlinear Constitutive Models.....	12
2.3.2 Application of ANN in Nanoindentation Nonlinear Constitutive Models .	14
CHAPTER 3 RESEARCH METHODOLOGY	15
3.1 Nanoindentation Testing	15
3.1.1 Introduction to Nanoindentation Testing.....	15
3.1.2 Surface Roughness.....	20
3.1.3 Nanoindentation on Fused Silica	20
3.1.4 Sample Preparation of Sand Grains	21
3.2 Finite Element Modeling.....	23

3.2.1	Constitutive Models	24
3.2.2	Convergence Study	25
3.2.3	FEM Model Verification.....	27
3.3	Artificial Neural Network (ANN) Modeling	29
3.3.1	Introduction to ANNs	29
3.3.2	Artificial Neural Network Structures.....	30
3.3.3	Developing an ANN for Nonlinear Material Behavior.....	36
3.3.4	Performance of the Developed ANN Model	40
3.3.5	Implementing the Nanoindentation Unloading Section in ANN.....	43
CHAPTER 4 RESULTS AND DISCUSSION		47
4.1	Nanoindentation Experiment Results.....	47
4.1.1	Fused Silica.....	47
4.1.2	Sand Grains.....	48
4.2	FEM Simulation Results	51
4.2.1	Effect of Indenter Tip Shape.....	54
4.2.2	Plastic Deformations and Stresses	55
4.2.3	Effect of Model Parameters	58
4.3	Artificial Neural Network Modeling Results	60
CHAPTER 5 CONCLUSION AND RECOMMENDATION.....		64
5.1	Summary and conclusion	64

5.2 Recommendation and Future Work	65
References.....	67

List of Figures

Figure 3- 1: Schematics of an indentation cross section after Oliver and Pharr (1992) ...	18
Figure 3- 2: Schematic load-displacement curve of a nanoindentation test after Oliver and Pharr (1992)	19
Figure 3- 3: Curve fitting result for determining Tip Area Function.....	19
Figure 3- 4: a. Polished sand grains in hardened epoxy resin, b. Surface of the single sand grains.....	22
Figure 3- 5: Surface topography (100 nm ² area) of the sample before indentation. Left, R _q =2.18 nm, Right, R _q =1.46 nm.....	23
Figure 3- 6: Yield surface of Modified Strucker-Prager/Plasticity Cap model in p-t plane. note that q=t in this paper. (From ABAQUS Users's Manual)	25
Figure 3- 7: Sensitivity analysis of FE results to sample dimensions.....	26
Figure 3- 8: 2D axisymmetric model of sample and conical indenter, the image is zoomed in from right to left.....	27
Figure 3- 9: Sensitivity analysis of FE results to mesh size	27
Figure 3- 10: FEM model verification, Nanoindentation on fused quartzs, 2-D Berkovich equivalent 70° indenter.....	28
Figure 3- 11: FEM model verification, Nanoindentation on fused quartzs, 2-D conical 55° indenter	29
Figure 3- 12: a. Schematics of a biological neuron cell after Moya and Irikura (2010) and b. a perceptron model after Messikh et al. (2017)	30
Figure 3- 13: ANN with m hidden layers and n nodes in each layer.....	32

Figure 3- 14: a. single feedback neuron, b. simple feedback neural network (after Zhang (2000)).....	36
Figure 3- 15: The truss used by Ghaboussi et al. (1998) to verify their ANN model.....	42
Figure 3- 16: Developed ANN model performance in comparison with the same model architecture proposed by Kim (2008)	43
Figure 3- 17: Performance of developed 4-layer ANN in predicting nanoindentation results	43
Figure 3- 18: Performance of ANN for predicting loading-unloading curve with different number of hidden layers with 5 nodes in each layer (H: number of hidden layers, N: Number of nodes)	45
Figure 3- 19: Performance of ANN for predicting loading-unloading curve with different number of hidden layers with 10 nodes in each layer (H: number of hidden layers, N: Number of nodes) – Note: 5-hidden layer network did not converge	46
Figure 4- 1: Representative result of nanoindentation test on Fused Silica.....	47
Figure 4- 2: Elastic modulus of Fused Silica for different indentation depths	48
Figure 4- 3: Representative result of nanoindentation test on sand grains	49
Figure 4- 4: Elastic modulus of sand grains for different indentation depths.....	49
Figure 4- 5: Berkovich indenter residual imprint on sand grain.....	50
Figure 4- 6: FE simulation of Fused Silica with a conical indenter and two constitutive models.....	53
Figure 4- 7: FE simulation of sand grain with a sharp Berkovich equivalent indenter and two constitutive models	53

Figure 4- 8: FE simulation of sand grain with a blunt Berkovich equivalent indenter and two constitutive models	54
Figure 4- 9: FEM simulation of nanoindentation on Fused Quartz using different indenter geometries.....	55
Figure 4- 10: Mises stress and sample deformation using: a. and b. sharp conical indenter, c. and d. blunt conical indenter	56
Figure 4- 11: Mises stress and sample deformation using: a. and b. sharp Berkovich indenter, c. and d. blunt Berkovich indenter.....	57
Figure 4- 12: Pile up and extreme residual deformation with low MDPC cohesion value (d=1.5 GPa).....	57
Figure 4- 13: Effect of Elastic modulus on load-displacement results of FE simulation using blunt conical indenter	59
Figure 4- 14: Effect of material cohesion (d) on load-displacement results of FE simulation using blunt conical indenter	59
Figure 4- 15: Loading curves of different values of Elastic modulus used in ANN training	61
Figure 4- 16: ANN model prediction of loading curves of different values of Elastic modulus compared with FE results.....	61
Figure 4- 17: Loading curves of different values of material cohesion used in ANN training	62
Figure 4- 18: ANN model prediction of loading curves of different values of material cohesion compared with FE results	62

Figure 4- 19: Predicted load-displacement curves with different values of Elastic modulus
..... 63

List of Tables

Table 3- 1: Typical activation functions used in ANNs	33
Table 4- 1: Initial model parameters for FEM	52

CHAPTER 1

INTRODUCTION

1.1 Problem statement

Behavior of material at different scales can sometimes be complex due to their nature and different methods of loads applied to the material. Although Fused Silica glass behaves as a brittle material under conventional flexural and uniaxial loading, it can behave differently under loading conditions that can prevent tensile stress such as nanoindentation tests. Unlike having the same atoms as crystalline Quartz which shapes sand grains, Fused Silica has amorphous molecular structure and this structure can result in lower Elastic modulus as well as compressibility to up to 20% under compression loadings. This behavior can also be seen in granular material such as powders or geomaterials. Soils also do not bear tensile stress but can show higher strengths when tensile stress is absent and densification behavior of soil is also observed under compressional loading. Different constitutive models have been used to describe this behavior of Fused Silica and some of these constitutive models have also been used in modeling soil behavior. Understanding the effect of different model parameters on behavior of material in micro as well as macro scale can help develop models that better capture the complex behavior of target material. This study aims to use Fused Silica as a basis of the investigation and further its application to Quartz and use the results to study the behavior of sand in macro-scale. To study various cases and understand the effect of different parameters, extensive parametric studies are needed which can be time consuming and computationally expensive. Thus, an Artificial Neural Network (ANN)

model was developed to learn from available data and predict material behavior in cases that have not been numerically simulated or experimentally studied. Using ANN for predicting nonlinear material behavior proved to be time efficient and accurate if the ANN model is properly structured and trained. One of the other advantages of ANN over other inverse analysis tools is that there is no need for prior determination of any equation for curve fitting of the material behavior. Using the combination of nanoindentation tests, finite element simulation and artificial neural network models can provide a robust system of analyzing material behavior that can also be used in viscoplastic and other categories of material behavior.

1.2 Research objectives and scope

This study aims to investigate the effect of different constitutive model parameters on micro-scale behavior of elastic plastic material especially Fused Silica and sand grains which have the same atomic combination. Performing nanoindentation tests on these materials provides a starting point of observing different behavior in micro scale compared to macro scale especially for Fused Silica. Additionally, finite element simulations of these material can provide a better understanding of how the material can be modeled using constitutive models and how different parameters of the constitutive modes can affect the results. Using Artificial Neural Network in addition to the studies mentioned before helps to investigate various properties that would be time consuming and inefficient if modeled with conventional methods. Therefore, a combination of these three methods shows to be promising in the area of mechanical behavior of material and will shed some light on the complications that can arise from different material behavior from micro to macro scale.

1.3 Organization of thesis

The present thesis consists of five chapters. After the introduction of the subject and the scope of the study in Chapter One, in Chapter Two previous work of researchers in areas related to the subject are presented. Since the proposed method consists of three main scientific methods, some of the reviewed material consists of only one or two of the methods and some a combination of these methods, and therefore of these sources are introduced. In Chapter Three the methodology of the research is introduced in three main parts: nanoindentation tests and their usage as well the theory behind the tests and sample preparation methods, FEM model and its convergence study and verification using other literature, ANN model development, verification and convergence studies as well as training and usage. Chapter Four consist of the results of the proposed methods in combination together. In Chapter Five the concluding remarks are made and some recommendations for future work in this area are presented.

CHAPTER 2

LITERATURE REVIEW

2.1 Nanoindentation Experiments

Material can behave differently at different scales due to their nature and construct as well as the types of applied loads. Granular materials like sand behave differently and like different forms of matter. They can behave like solids with a large amount of void space in them and can support load, but unlike solids they cannot bear tensile stress. Like liquids they can flow and take the shape of their container but unlike liquids they have shear strength. They consist of discrete elements like gases however unlike gases they are not significantly compressible. This complex behavior can be studied and understood better using micro-scale (continuum in case a single grain of sand) to macro-scale (discrete in case of the granular material) mechanical investigations. The behavior of granular material at macro-scale is directly influenced by the mechanical properties of the elements constructing them at micro-scale such as the Young's modulus, fracture toughness, surface roughness, hardness, and load-deformation behavior of individual grains. The same scaling and analogy can also be used at a different level for amorphous material like Fused Silica, as the atomistic characteristics of the molecular and non-crystalline structure is the source of the micro-scale behavior of this material. For instance, as the atoms are dislocated and localized densification occurs under uniaxial microscale loading, plastic deformation at this scale happens but at a larger scale the insufficient tensile forces between atoms results in crack growth and as a result brittle behavior of this material at macro-scale. The shear failure due to developed slip surface is

a common factor of failure in granular material in continuum level. It is interesting to see that the same mechanism can cause the failure of amorphous material in micro-scale. Instrumented indentation of material namely nanoindentation has been used widely in the past three decades to investigate different material behavior such as elastoplastic or viscoelastic at micro and nano scale. The scale of loads and displacement in these tests are in the order of microNewton and nanometer or micrometer. The scale of the analyzed material using nanoindentation method is correlated mainly to the indentation depth. This is not the only quantity that depends on the indentation depth: Since the contact area in nanoindentation is too small to directly measure, it is calculated using correlations with the indentation depth. Oliver and Pharr (1992) proposed a method to use nanoindentation load-displacement response to calculate Young's modulus of the material. They used the Berkovich indenter to characterize different material such as fused silica, aluminum, quartz, etc. by calculating their Young's modulus and hardness using their proposed method. In recent years many scientists have used nanoindentation tests to study the size effect on plastic deformation of material in continuum level. Al-Rub and Voyiadjis (2004) proposed an analytical method to show that continuum plastic behavior can be derived from micro-scale measurable parameter and showed that length scale parameters can be identified using this method. Dutta and Penumadu (2007) measured the elastic modulus and hardness of sand grains using nanoindentation. Daphalapurkar et al. (2011) used nanoindentation to identify Young's modulus, hardness, and fracture toughness of individual sand grains and used inverse problem solving methods as well as statistical data analysis to assess the overall mechanical properties of sand grains to be used in mesoscale studies. Wang et al. (2011) also used the same approach in addition to X-Ray

Diffraction (XRD) technique to study mechanical and crystal properties of sand grains by means of nanoindentation.

A handful of studies have also been performed to investigate the densification of fused silica under nanoindentation loading. Xin and Lambropoulos (2000) and Kermouche et al. (2008) used the results of nanoindentation tests on fused silica in combination with FE analysis to derive a new constitutive model for capturing indentation-induced densification of this material. Bruns et al. (2017) used the same approach and introduced another constitutive model for plastic deformation and densification as well as indentation cracking of fused silica. Additionally, Torres-Torres et al. (2010) studied the effect of indenter tip geometry, shape and bluntness on nanoindentation results and determined the yield stress of fused silica in von Mises stress space.

2.2 Constitutive Models

Considering the densification behavior of Fused Silica, researchers have tried to use different constitutive models to describe the plastic flow in this material. Marsh (1964) started with showing the evidence of plastic flow in Fused Silica using the results of various indentation hardness and scratch tests with low-amplitude loads. Even though the effect of compaction of different glass material were addressed and confirmed that there are different amounts of compaction for different glass material, the effect was thought to be negligible thus only volume-conservative plastic flow was assumed to play the role in plastic deformation of Fused Silica.

As mentioned before, the development of shear slip surface in amorphous material can have the same mechanism in granular material, which is the subject of the studies by

many researchers. Li et al. (2015) studied the failure of amorphous granular pillars under compressional loading and Bouil et al. (2014) observed the plastic flow and shear failure in soft glassy material. Maloney et al. (2006) also observed developed shear failure planes in molecular simulations of amorphous systems.

Lambropoulos et al. (1996) took into account the effect of densification and introduced a new constitutive model assuming that the incremental plastic strain consists of both densification (caused by volumetric strain) and shear flow. Even though the amorphous nature of Fused Silica implies that it is isotropic and the yield behavior will be governed by three stress invariants, Lambropoulos et al. (1996) assumed that the yield condition depends on only first two stress invariants. They also assumed that the yield function has linear dependency on hydrostatic pressure and shear stress, resulting in:

$$f(\sigma_{ij}) = -p + \zeta q - \sigma_0 \equiv 0 \quad (2-1)$$

in which p is hydrostatic pressure, q is equivalent shear stress ($q = \sqrt{s_{ij}s_{ij}/2}$), σ_0 is yield stress, and ζ is an arbitrary positive material constant giving the contribution of shear in triggering and retaining densification.

Later on, Xin and Lambropoulos (2000) proposed another yield criteria for behavior of Fused Silica considered the contribution of shear and hydrostatic pressure in yielding as a variable:

$$f(\sigma_{ij}) = -\alpha p + (1 - \alpha)q - Y \equiv 0 \quad (2-2)$$

in which $0 \leq \alpha \leq 1$ is a constant determining the contribution of shear and hydrostatic pressure in yielding, and Y is the yield stress which is different than σ_y under uniaxial

tension or compression. As it can be seen in Eq. 2, if $\alpha = 0$, the equation turns into shear flow theory, and if $\alpha = 1$, the yielding is done under pure hydrostatic condition. By fitting the experimental indentation curves to the results of numerical modeling, Xin and Lambropoulos found the values of the above parameters to be $\alpha = 0.6$ and $Y = 9.4$ GPa.

These simple criteria were further developed and modified by other researchers. The reasons for these further developments are first, linearity of these equations with the associate flow rule hypothesis does not take into account the dependence of direction of plastic strain rate on either hydrostatic pressure or shear stress; and second, the densification-induced hardening behavior which has been observed by Perriot et al. (2006) for Fused Silica needs to be considered in the constitutive model. Perriot et al. (2006) used Raman microspectroscopy to characterize the plastic behavior of amorphous silica. They used the results of Diamond Anvil Cell experiments to show the densification-induced hardening of Fused Silica. Using the test results, they illustrated the densified area mapping showing that the material can be densified to up to 20% gradually as the load increases. In the case of confined boundary conditions, while the volume-conserving deformation occurs under shear flow, densification-induced hardening is caused by hydrostatic pressure and it is the most dominant cause of plastic deformation. On the other hand, if the material is not confined, it has been observed that the shear deformation is the major cause of plastic behavior compared to densification. In case of nanoindentation tests, the densification is caused indirectly under the indenter tip.

Kermouche et al. (2008) proposed that, since the plastic behavior of Fused Silica has a strong dependency on hydrostatic pressure, the behavior has a lot of similarities to

geomaterial or powders. However, it was assumed that there is no frictional behavior in Fused Silica thus maintaining the associate plasticity. Furthermore, the effect of negative pressure was neglected. Due to the lack of experimental data, Kermouche et al. (2008) did not consider shear hardening for their constitutive model and assumed only densification-induced hardening for their model. Therefore, a criterion consisting of a simple von Mises criterion for negative hydrostatic pressure and an ellipse criterion for positive hydrostatic pressure was introduced as:

$$f(\sigma_{ij}) = \begin{cases} \left(\frac{q}{q_c}\right)^2 + \left(\frac{p}{p_c}\right)^2 - 1 & p > 0 \\ q - q_c & p < 0 \end{cases} \quad (2-3)$$

where p_c is hydrostatic plastic limit in pure hydrostatic state, and q_c is shear limit in pure deviatoric state. As discussed before, now the direction of plastic strain rate depends on hydrostatic pressure:

$$\dot{\varepsilon}_{ij}^p = \dot{\lambda} \left(3s_{ij} - \frac{2q_c^2}{3p_c^2} p \delta_{ij} \right) \quad (2-4)$$

It can be seen that the plastic densification only occurs in pure hydrostatic state. Due to the lack of experimental data, Kermouche et al. (2008) did not consider shear hardening for their constitutive model and assumed only densification-induced hardening for their model. The densification-induced hardening was assumed to have a linear relationship with the hydrostatic pressure, in which the increase in volumetric strain causes a linear increase in hydrostatic plastic limit p_c :

$$p_c = \xi \varepsilon_m^p + p_{c0} \quad (2-5)$$

Kermouche et al. (2008) calibrated the values for the parameters introduced in the model by fitting the numerical analysis results to the experimental data: $E = 72 \text{ GPa}$, $\nu = 0.18$, $p_{c0} = 11.5 \text{ GPa}$, $\xi = 100 \text{ GPa}$, and $q_c = 6.5 \text{ GPa}$.

Another effect of hydrostatic pressure on material properties of Fused Silica was changing of Young's Modulus and Poisson's ratio which was studied by Keryvin et al. (2014). They also observed the saturation of densification in high pressure. In recent studies, Bruns et al. (2017) and Kermouche et al. (2008) used a modified Drucker-Prager Cap model to capture both elastic-plastic response and densification under indentation loading. They used ABAQUS FEM analysis as well as nanoindentation experimental results to find the model parameters that are suitable for Fused Silica. They also captured the crack growth inside the material using cohesive zone and concluded that densification under the indenter tip causes slower crack growth and propagation. The suggested elliptical yield surface equation by Bruns et al. is:

$$q = \sqrt{d^2 \left[1 - \left(\frac{p}{p_c} \right)^2 \right]} \quad (3-6)$$

where d is the yield strength under pure shear and the rest of the parameters have been described before in this text. The densification-induced hardening is also implemented using Eq. 5 for only 1% volumetric strain. The values of the parameters that result in the best fit of numerical and experimental results are $d = 7.5 \text{ GPa}$, $p_c = 11.5 \text{ GPa}$, $p_c(1\%) = 12.5 \text{ GPa}$, and von Mises yield strength is 7.5 GPa .

2.3 Artificial Neural Network (ANN) Models

2.3.1 ANN for Nonlinear Constitutive Models

Constitutive models that can accurately describe and predict complex nonlinear material behavior at different length scales usually have many parameters that need to be calibrated using experimental data. Classical constitutive models can utilize a small range of variables due to complexity that adding more coefficients causes. To expand their usage, adding even a single parameter or coefficient to an older constitutive model requires an extensive amount of experiments and numerical simulations to achieve a high accuracy. Considering the cost and time for re-calibrating and verifying a newly introduced constitutive model, it is usually more efficient to use less parameters and sacrifice partial accuracy to achieve acceptable results. This is where the efficiency of Artificial Neural Network (ANN) modeling is most evident. ANN models can provide better accuracy and expand the usage of traditional constitutive models to better predict complex material behavior. This is achieved by simply adding more neurons to the model and adjusting their weights in contribution to the output to achieve higher accuracy. This method is inspired by how nature adapts itself to different conditions. ANN models are trained using experimental results as well as verified and known to be accurate numerical simulation results. Once the accuracy of a well-trained model is ensured, it can be used to predict material behavior under different loading conditions that were not studied using experiments or numerical simulations.

ANN models that are accurately trained can also be used in a variety of inverse analysis problems to extract material properties using experimental results. This can be achieved by properly constructing the model to have variables that are suitable for inverse analysis

and by proper relations between input and outputs of the model. This is significant because studying an unknown material using nanoscale testing methods such as nanoindentation can sometimes be influenced by external factors such as noise in the data originating from vibrations in the environment. In the case of nanoindentation tests, only a limited number of material properties, i.e. Young's modulus and hardness, can be obtained from experiment thus in research nanoindentation tests need to be combined with FEM simulations to better characterize the material under study in form of constitutive model parameters. This method can be inefficient since every small change in the finite element model requires a new run of the model to see the effects of that change. Thus an ANN model can be used to study the effect of these changes in a more accurate and efficient way. Different variables can be added to the ANN model to study the influence of the nanostructure on the overall behavior of the material.

There has been no studies that utilize ANN models to investigate the material response of different forms of silica and the constitutive models used to describe their behavior.

Therefore, studies over the last two decades that have used ANN modeling to predict nonlinear behavior of material in general will be addressed. Sidarta and Ghaboussi (1998) used ANN to extract nonlinear constitutive behavior of sand under triaxial compression loading and in their other publication Ghaboussi and Sidarta (1998), they introduced a new method called Nested Adaptive Neural Network (NANN) to also model the undrained and drained behavior of sand in triaxial tests. Fu et al. (2007) also used the same approach for analysis of results of laboratory tests on geomaterial and called it self-learning simulation method.

2.3.2 Application of ANN in Nanoindentation Nonlinear Constitutive Models

To extract material properties from nanoindentation using ANN, a well-trained ANN model can be used to find the best combination of material properties that yield a load-displacement curve that is in the best agreement with experimental results. Among the first researchers who used ANN in nanoindentation response of material of films and substrates were Mulinia et al. (2002) who performed a comprehensive study consisting of 2D and 3D FE analysis as well as nanoindentation tests on annealed copper and used ANN models to generate load-displacement curves of nanoindentation tests on a variety of materials and indenter geometries. After training the models, their prediction capability was tested against FE simulation results that were not used in ANN training. Huber et al. (2002) used the same approach to study plastic behavior of indentation of aluminum films. Tho et al. (2004) in addition to using load-displacement curves, used the area under the curves as input parameters to train two consecutive ANN models. Tyulyukovskiy and Huber (2006) developed a viscoplastic model and simulated nanoindentation and used the FE results to train the ANN model with parameters including yield stress, the initial slope of work hardening, and maximum hardening stress of the equilibrium response as well as elastic deformation. Haj-Ali et al. (2008) used only the monotonic loading part of the nanoindentation load-displacement curve to train the ANN model that used dimensionless input and output variables. They performed nanoindentation tests on copper films on silicon substrates.

CHAPTER 3

RESEARCH METHODOLOGY

3.1 Nanoindentation Testing

3.1.1 Introduction to Nanoindentation Testing

Nanoindentation tests have been used in many different areas to study mechanical properties of material mostly when samples are small and conventional tests are not possible to be performed on them such as thin films, when enough sample is not available, or on devices such as MEMS and NEMS. The basic idea behind nanoindentation is measurement of reaction force and displacement of an indenter when it is being pushed into the surface of the sample by the actuator. It can be performed load-control or displacement-control. In load-control method, a time history of force vs. time is used to apply force on the surface of the sample using the indenter, while the displacements of the indenter is being measured. The device tries to keep the reaction force close to the loading time history. In displacement-control method, a known displacement time history is used to move the tip of the indenter inside the sample while measuring the reaction forces applied to the indenter from the sample. In most cases deformations caused by an indentation test are elastic-plastic and there is residual deformations left on the location of indentation. The two major mechanical properties extracted from nanoindentation tests are Young's modulus (E) and hardness (H). One of the major parameters in an indentation test is the contact area which is measured directly in large scale indentations but since the residual imprint of the indenter in nanoindentation is very small and cannot be measured directly, the contact area is

calculated in correlation with indentation depth since the geometry of the indenter is known. But this method needs calibration as the indenter usually has some imperfections in its shapes and it also can become blunt over time as it is used for many tests.

Therefore, to calibrate the device and the function that is used to correlate the indentation depth to contact area, a tip area function (TAF) is used. To obtain this function, some indentation tests are performed on a material with known values of elastic modulus and hardness, measuring the load-displacement curve from the tests. By fitting the calculated mechanical properties to known mechanical properties, the parameters of the tip area function are calculated which then can be used to calculate contact area with respect to the indentation depth. Figure 3- 1 illustrates the schematics of the cross-section of an indentation and different parameters used in the method proposed by Oliver and Pharr (1992) to calculate elastic modulus and hardness. Total displacement in the indentation loading is written as:

$$h = h_c + h_s \quad (3-1)$$

where h_c is called the contact depth and h_s is the displacement of the surface of the sample at the perimeter of the contact. During the loading phase, the indentation force will reach the maximum value of P_{max} and the indentation depth will have a value of h_{max} . Assuming the indenter tip has a conical shape with a known centerline-to-face angle, the contact area can be calculated as a circle with radius a . After the unloading is finished, residual deformation on the surface of the sample will have depth of h_f .

Even though the material used for the indenter has a significantly high modulus and its deformations are negligible related to the deformations of the sample, to take into account

the deformation of the indenter, a value called “reduced modulus” (E_r) is defined as below:

$$\frac{1}{E_r} = \frac{1-\nu^2}{E} + \frac{1-\nu_i^2}{E_i} \quad (3-2)$$

where E and ν are Young’s modulus and Poisson’s ratio of the sample and the subscript i indicates the properties of the indenter.

A typical response of an indentation test is schematically shown in Figure 3- 2. To calculate the reduced modulus using the load-displacement curve, as proposed by Doerner and Nix (1986), the slope of the upper one-third section of the unloading curve (S) is used:

$$S = \frac{dP}{dh} = \frac{2}{\sqrt{\pi}} E_r \sqrt{A} \quad (3-3)$$

where A is the imprinted area of the elastic contact. Eq. (3-3) is derived from elastic contact theory by Bulychev and his coworkers (1975) originally for conical indenters, it was shown later by Pharr, Oliver, and Brotzen (1992) that this equation can be applied to any indenter with the shape that can be described as a body of revolution of a smooth function around an axis of symmetry and with an acceptable approximation for other indenters with pyramidal shape.

To calculate the contact area, a function that correlates contact depth to contact area is used which can be unique to the shape of the indenter and can be determined either with functions introduced in the literature or by curve fitting technique. Thus a series of nanoindentation tests with different maximum depths was performed on Fused Silica

provided by Hysitron Company with the declared Reduced Elastic Modulus $E_r = 69.6$ GPa and hardness $H = 9.25$ GPa to define the Tip Area Function as shown in Figure 3- 3. The equation that was used is defined as:

$$A = C_0 h_c^2 + C_1 h_c + C_2 h_c^{1/2} + C_3 h_c^{1/4} + C_4 h_c^{1/8} + C_4 h_c^{1/16} \quad (3-4)$$

With the contact area known, hardness can be calculated as:

$$H = \frac{P_{max}}{A} \quad (3-5)$$

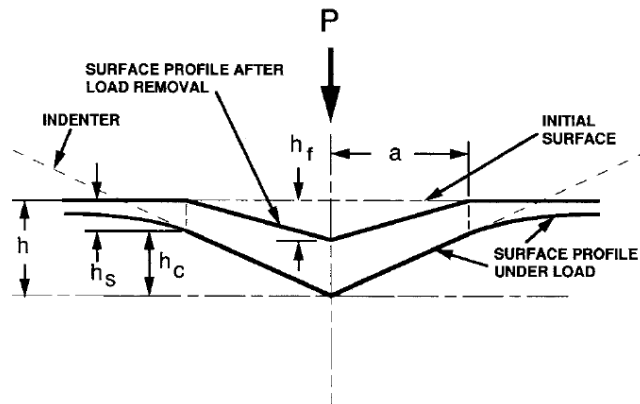


Figure 3- 1: Schematics of an indentation cross section after Oliver and Pharr (1992)

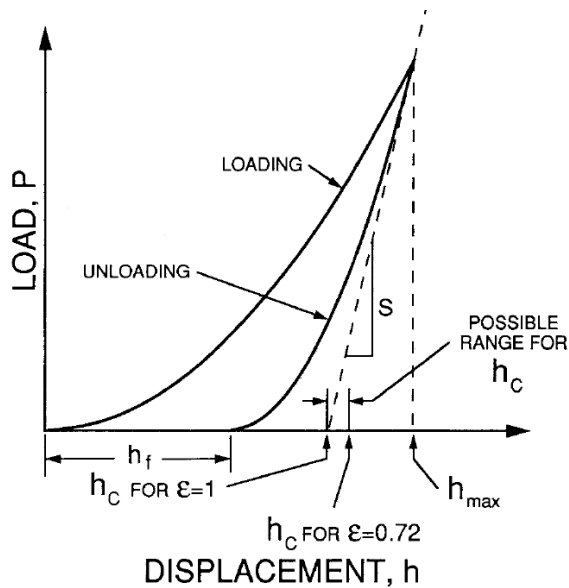


Figure 3- 2: Schematic load-displacement curve of a nanoindentation test after Oliver and Pharr (1992)

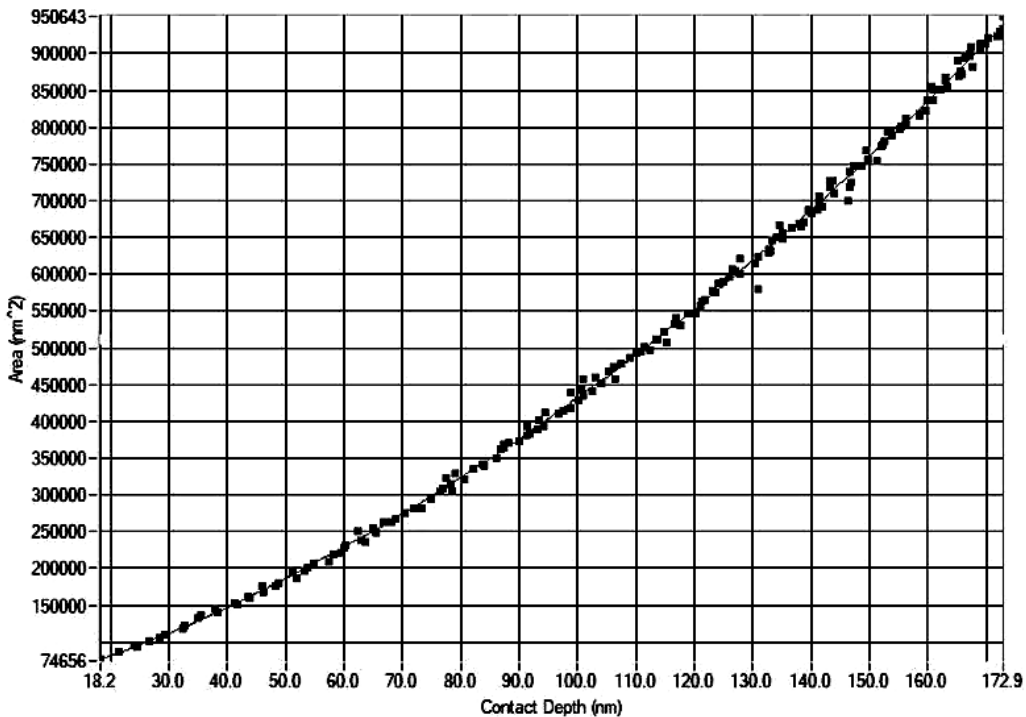


Figure 3- 3: Curve fitting result for determining Tip Area Function

3.1.2 Surface Roughness

One of the important assumptions in all the equations presented in previous section is that the surface of the sample is completely flat. Therefore, one of the most important parameters that can affect nanoindentation test results is surface roughness of the sample. If the surface of the sample is rough and has bumps the contact depth can be mistakenly selected therefore resulting in an inaccurate contact area. Thus, the surface of the sample need to be prepared and polish and its surface roughness measured prior to nanoindentation tests. One of the methods to measure surface roughness is calculating the root mean square (RMS) of surface heights, R_q , along the sampling surface:

$$R_q = \sqrt{\frac{1}{A_s} \iint z^2 dA} \quad (3-6)$$

where A_s is the sampling surface and z is the height of the sample at different locations.

3.1.3 Nanoindentation on Fused Silica

For all the nanoindentation tests on the samples the Hysitron¹ TI Premier Nanoindentation device located at the Soil Mechanics Laboratory at Department of Civil Engineering of University of Nebraska Lincoln was used.

for means of device calibration was used to study the nanoindentation behavior of this material. No sample preparation was needed. A series of 256 displacement-control tests with maximum displacement of 250 nm corresponding to the maximum load capacity of the device (11000 μN) were performed on different locations on the sample surface to extract the load-displacement curves as well as device calibration. Half of the

¹ www.hysitron.com

mentioned tests were performed using a Berkovich indenter tip with total angle of 142.3° and nominal radius of approximately 100 nm (called “Berkovich indenter” in the rest of the text) and the rest were performed using a conical indenter tip with the face-to-centerline angle of 45° and tip radius of $1.4 \mu\text{m}$ (called “conical indenter” in the rest of the text).

3.1.4 Sample Preparation of Sand Grains

The sand grains used for the tests were the standard ASTM 20-30 C778 purchased from U.S. Silica Company. The sand grains consist of %99.8 SiO_2 as mentioned in the product catalog. To prepare the sample a small amount of sand grains were poured into Allied² 1" diameter cylindrical plastic mounting cup and submerged with approximately 1/3" height of acrylic resin purchased from EMS³ under the name of LR White Resin. After temperature treatment of the epoxy resin to harden, the sample was extracted from the mounting cup and was mounted in the E-PREP 4TM Grinder/Polisher with PH-4ITM Power Head manufactured by Allied Company. The sample was then grinded and polished using the following (in order) grades of Silicon Carbide sandpapers and Alumina Powder Suspensions applied on SPEC-Cloth produced by Allied company:

- 320 Grit
- 600 Grit
- 800 (P-2400) Grit
- 1200 (P-4000) Grit
- 2500 Fine Grit
- $1 \mu\text{m}$ Alumina Powder
- $0.3 \mu\text{m}$ Alumina Powder
- $0.05 \mu\text{m}$ Alumina Powder

² www.alliedhightech.com

³ www.emsdiasum.com

The final polished sample is shown in Figure 3- 4-a and the microscopic image of the surface of the sample is shown in Figure 3- 4-b. To measure the roughness of the polished samples, surface topography of the sample was obtained using the indenter probing method in an area of $10\ \mu\text{m}$ by $10\ \mu\text{m}$. Figure 3- 5 shows the topography of the locations on sand grains indicated by red dots in Figure 3- 4-b. The RMS roughness of the scanned surfaces are significantly low averaging less than $2.5\ \text{nm}$ which indicates a very good polished surface.

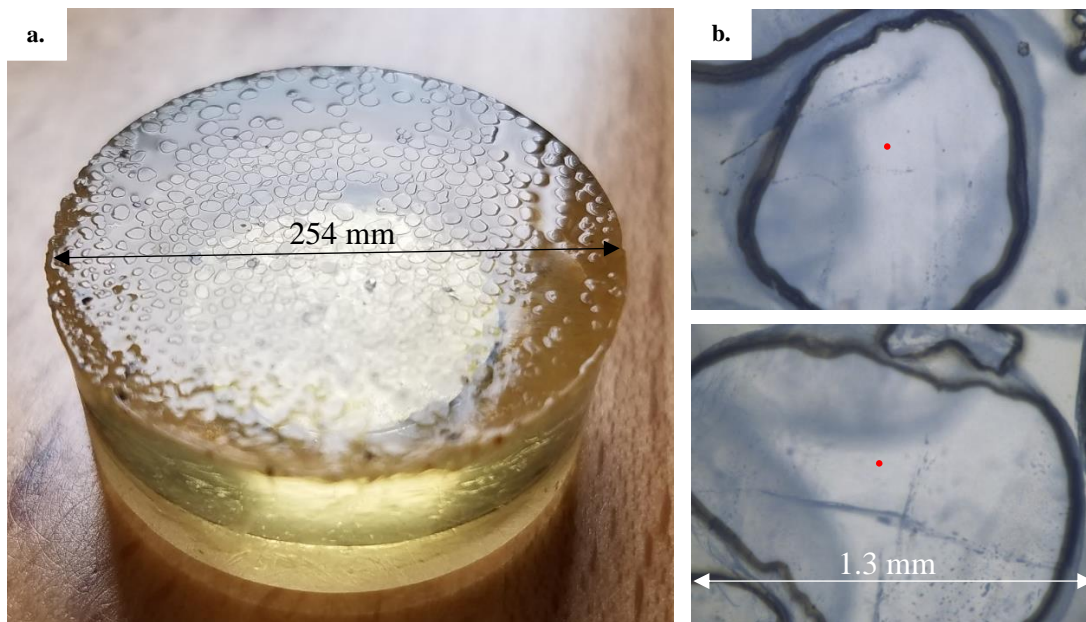


Figure 3- 4: a. Polished sand grains in hardened epoxy resin, b. Surface of the single sand grains

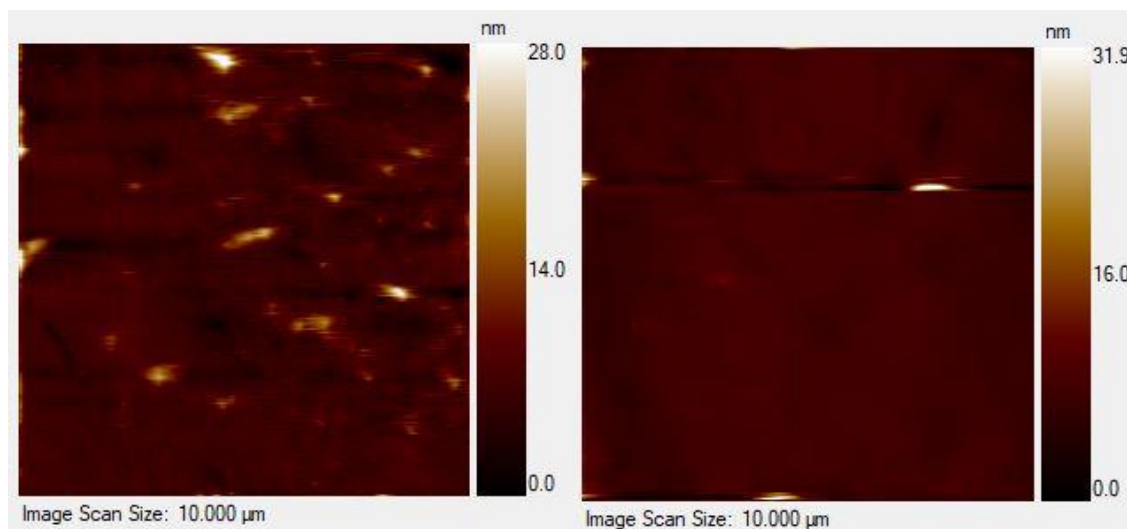


Figure 3- 5: Surface topography (100 nm^2 area) of the sample before indentation. Left, $R_q=2.18 \text{ nm}$, Right, $R_q=1.46 \text{ nm}$

3.2 Finite Element Modeling

A series of numerical analyses were performed in order to compare the response of the material using different plasticity constitutive models. For model verification, the results were compared to experimental and numerical results from available literature. The commercial FEM software Simulia ABAQUS 6.12-3 was used for these analyses. The models consist of 2-D four-node bilinear axisymmetric quadrilateral with reduced integration elements (CAX4R) to model the sample and a rigid surface to model the indenter.

Boundary conditions for the model are fixed in horizontal (x) and vertical (y) direction at the bottom of the model, fixed only in x direction on the axis of symmetry, and free on the right side and top of the model. The surface of the indenter is fixed related to a Reference Point thus the displacement of the Reference Point corresponds to the displacement of the indenter. Since body forces are negligible in this case, the initial conditions did not consider the weight of material.

3.2.1 Constitutive Models

The Modified Drucker-Prager/Cap Plasticity model is typically used for geomaterial since their yielding behavior depends on the hydrostatic pressure. The cap yield surface makes the model able to capture hardening behavior due to plastic compaction as well as controlling volume expansion that happens due to shear failure. This yield surface is comprised of a shear failure segment and a cap segment. The formulation of this constitutive model in ABAQUS is based on the $p - t$ plane, in which p is the hydrostatic stress and t is the deviatoric stress measure defined as:

$$t = \frac{q}{2} \left[1 + \frac{1}{K} - \left(1 - \frac{1}{K} \right) \left(\frac{r}{q} \right)^3 \right] \quad (3-1)$$

in which q is the Mises equivalent stress $q = \sqrt{\frac{3}{2} s_{ij} s_{ij}}$, r is the third invariant of

deviatoric stress $r = \left(\frac{9}{2} s_{ij} s_{kl} s_{kl} \right)^{\frac{1}{3}}$, and K is a material parameter depending on

temperature and pre-defined field variables. The shape of the yield surface can be seen in Figure 3- 6. It is mentioned in ABAQUS Users's Manual that this measure of stress is used because it provides a more consistent explanation of deviatoric stress in tension and compression in deviatoric plane and providing a more flexible fitting of experimental data and good approximation to the Mohr-Coulomb surface. Since in all the previous paper, the dependency on third deviatoric stress was not considered, we can assume that $K = 1$. In this case, $t = q$. It should be noted that in order to make sure that the yield surface is always convex, $0.778 \leq K \leq 1.0$.

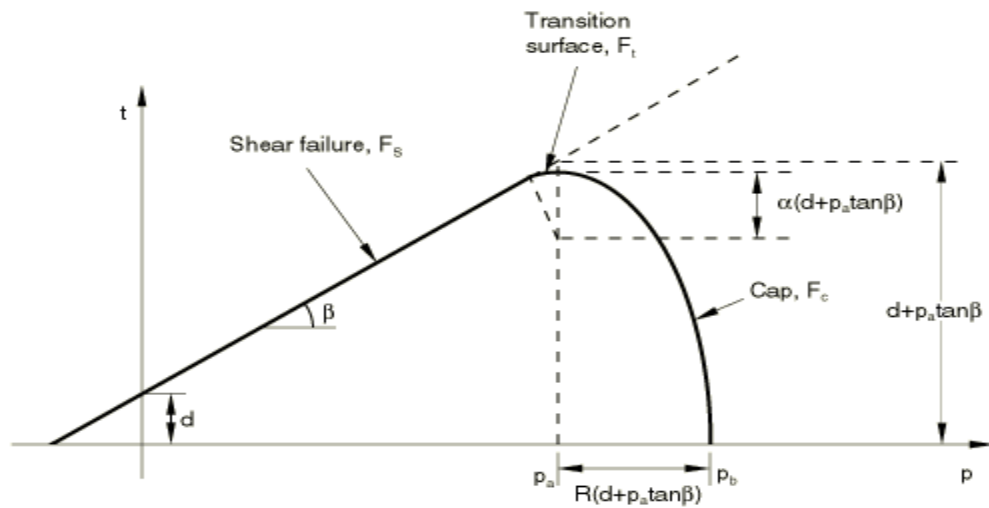


Figure 3- 6: Yield surface of Modified Drucker-Prager/Plasticity Cap model in p-t plane. note that $q=t$ in this paper. (From ABAQUS Users's Manual)

An elastic-plastic constitutive model was also used in the FE simulations in order to capture the difference and compare the results of Drucker-Prager/Cap model. The only inputs of this model consist of Young's modulus, Poisson's ratio, density and yield stress.

3.2.2 Convergence Study

It is important that the boundaries of the sample in the FE simulation do not affect the results. Therefore, a series of analysis were performed to find an acceptable sample dimension. Since the maximum indentation depth in this study was 500 nm, a sample with dimensions of $5 \times 5 \mu\text{m}$ was used as a starting point and multiple numerical simulations were run while increasing the sample dimensions until no significant change was noticed in the results as shown in Figure 3- 7. The sample dimensions were $50 \times 50 \mu\text{m}$, which is proved to be big enough to avoid boundary effects on the results. The model mesh and size can be seen in Figure 3- 8.

To find the adequate mesh size for the model, a convergence study was performed by decreasing the size of the elements in the vicinity of the indenter tip and the results were compared. A finer mesh was used near the indenter to achieve more accurate results.

Figure 3- 9 presents the results of the convergence study, therefore the chosen element dimensions near the indenter tip was $0.1 \mu\text{m}$. The numerical simulation was run in Update Lagrangian reference frame and nonlinear deformation was assumed.

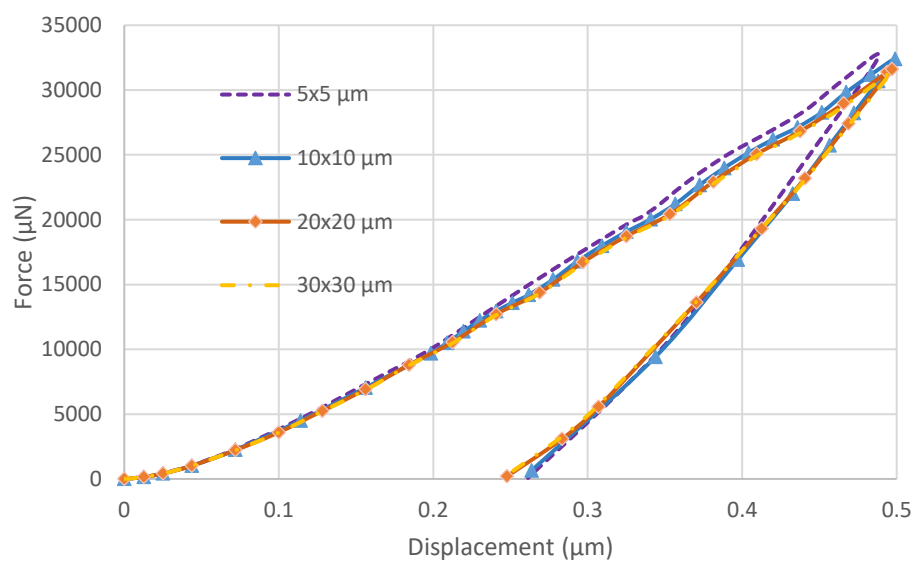


Figure 3- 7: Sensitivity analysis of FE results to sample dimensions

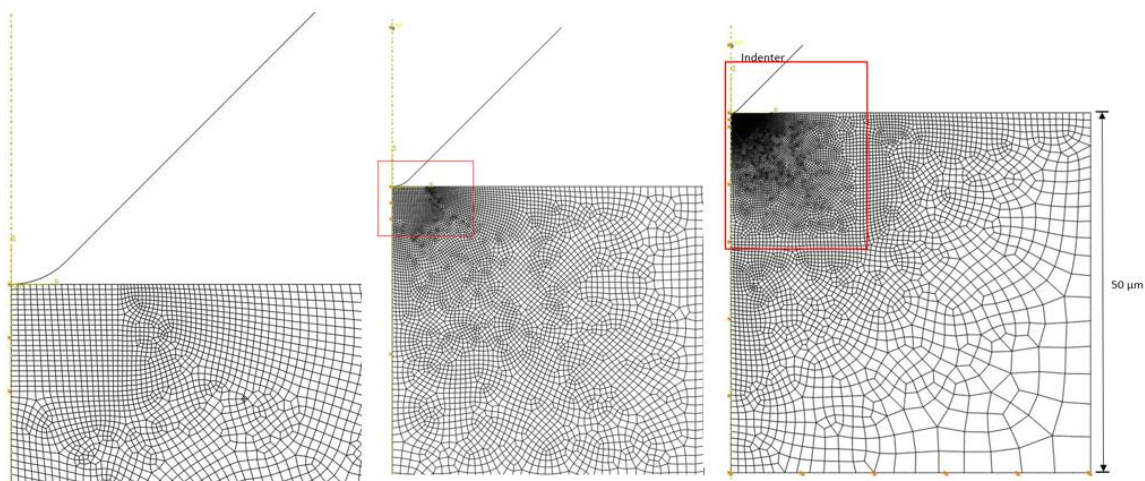


Figure 3- 8: 2D axisymmetric model of sample and conical indenter, the image is zoomed in from right to left

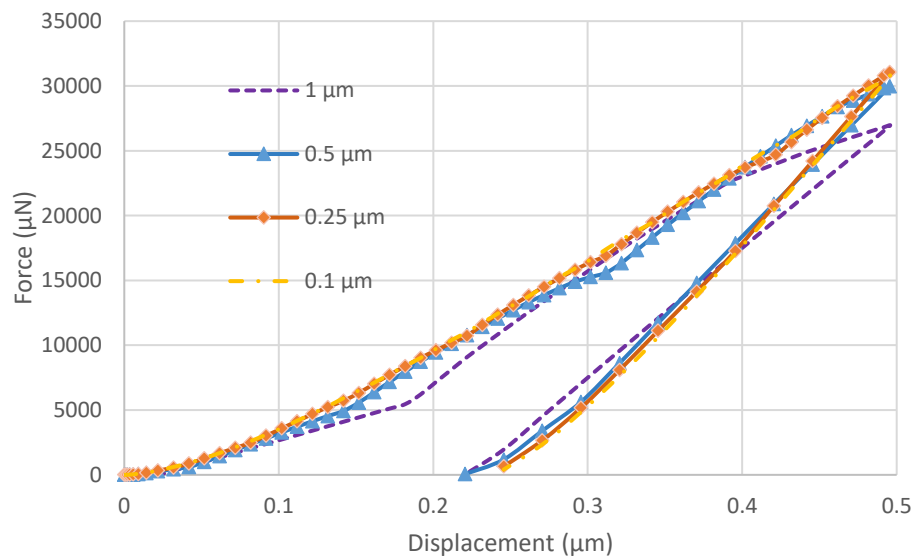


Figure 3- 9: Sensitivity analysis of FE results to mesh size

3.2.3 FEM Model Verification

After the convergence study and determination of the sample size, nanoindentation finite element model for the conical indenter was verified against the results of Bruns et al.

(2017) study as they used a 55° half-angle conical indenter and it can be assumed close to the 45° indenter used in this study, and for modeling the Berkovich indenter results from Kermouche et al. (2008) was used as in their paper an equivalent 70° half-angle conical indenter was used to successfully replicate the nanoindentation test results from a Berkovich indenter. The same approach was taken in the present study. Nanoindentation load-displacement curves were normalized since the details of indentation depth was not presented by Bruns et al. (2017) and for other results as well, for the sake of consistency.

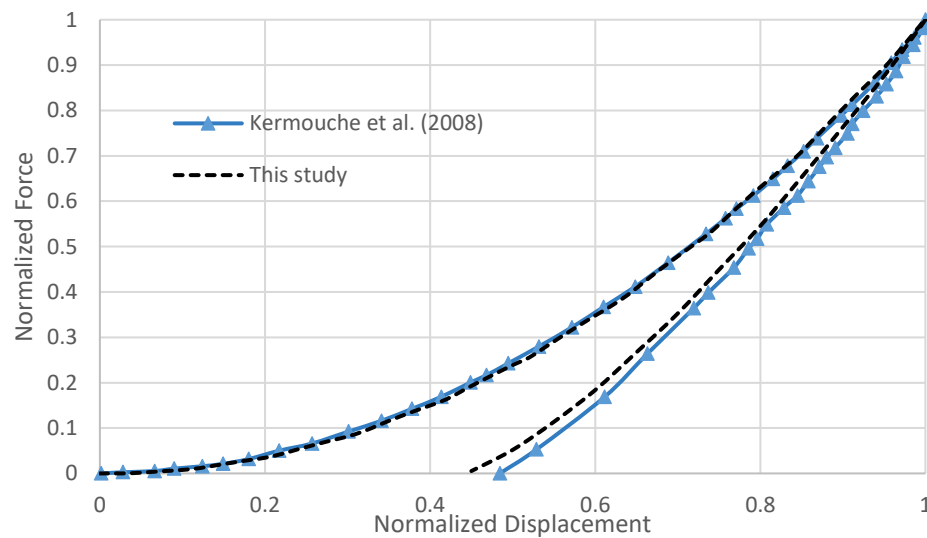


Figure 3- 10: FEM model verification, Nanoindentation on fused quartz, 2-D Berkovich equivalent 70° indenter

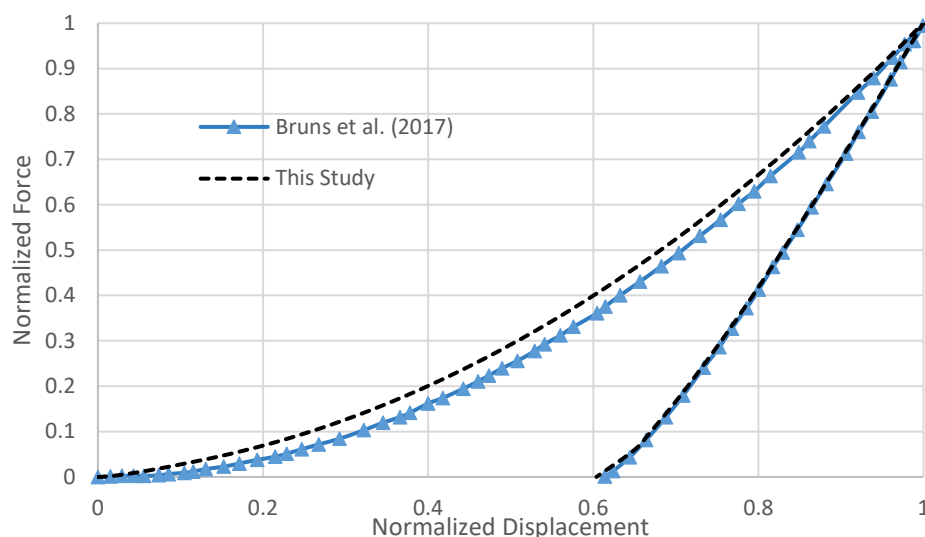


Figure 3- 11: FEM model verification, Nanoindentation on fused quartz, 2-D conical 55° indenter

3.3 Artificial Neural Network (ANN) Modeling

3.3.1 Introduction to ANNs

Artificial Neural Networks (ANNs) has been used for many decades in many scientific fields such as economics and finance, medicine, risk analysis, meteorology, computer science, robotics and Artificial Intelligence, civil engineering, and so on. In addition to scientific fields, ANNs have also been used commercially. Artificial Neural Networks (ANNs) are computerized way of how the human brain processes information; they are computer programs that can be trained, like humans, to detect and learn from patterns and relationships, that may be hidden or obvious, in existing data. There is significantly less number of neurons in an ANN system compared to human brain, but the mechanism is inspired by how human brain works: a system of interconnected neuron cells that pass signals through one another. As shown in Figure 3- 12-a, a neuron cell consists of four

major parts: dendrites that receive signals from other neurons, cell body that sums up all incoming signals into the cell, axon that lets the output signal out of the cell if it reaches a certain threshold, and synapses that pass the signal to other neurons depending on the strength of the connection (i.e. the weight of the connection). The strength of these connection is not constant and can increase or decrease. This simple neuron was first developed by McCulloch and Pitts in 1943 and despite the years passed, it is still one of the most used concepts in ANN. However, it should be noted that in their model a simple step function was used but other functions, as described in later sections, can also be used as the transformation function. This analogy in ANNs is called a perceptron (Figure 3-12-b) which is connected to other nodes to form the whole ANN structure which is discussed in the following sections.

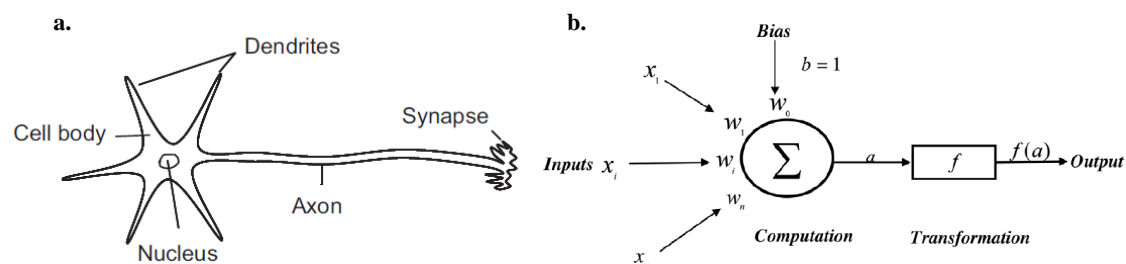


Figure 3- 12: a. Schematics of a biological neuron cell after Moya and Irikura (2010) and b. a perceptron model after Messikh et al. (2017)

3.3.2 Artificial Neural Network Structures

3.3.2.1 Function of a Single Artificial Neuron

In the simplest artificial neuron, a scalar input x is sent to the neuron and is multiplied by the neuron weight w to calculate the neuron output y using the activation (or transformation) function. Thus the output will be $y = f(wx)$. In some cases to get a more

acceptable output, a bias is added to the equation forming the output as $y = f(wx + b)$.

The values of weight and bias (w and b) are then adjusted to get the most accurate output.

The input of the activation function can also have a more complex form rather than

linear, such as quadratic, forming the output as $y = f(wx^2 + b)$ or other complex forms

however the linear form is mostly used. The next level of complexity for a neuron is

changing the scalar input to an array input consisting of $x_i, 1 \leq i \leq n$ and $w_i, 1 \leq i \leq n$

therefore calculating the output as $y = f(\sum wx + b)$ which is also illustrated in Figure 3-

1-a.

3.3.2.2 Construction of a Neural Network

Connecting the single neurons explained in previous section forms a neural network in a

way that the output of a single neuron will be the input of every other neuron in its next

layer. There are three main layers in computational neural networks: the input layer with

values x_1 to x_n , a hidden layer with nodes that receive the input from another layer,

multiplies each input by its designated weight and adds bias, and the output layer which

is the calculated values of the combination and transformation of inputs, weights and

biases through activation functions. There can be multiple hidden layers in a neural

network to make it capable of predicting more complex and nonlinear data. For instance,

a neural network with two hidden layers will ultimately be called a four-layer neural

network. The number of nodes in a layer is determined either by the architect of the

network or by adaptive learning. A schematic view of an ANN with n inputs, m number

of hidden layers each containing n nodes, and n outputs is shown in Figure 3- 13. It

should be noted that the number of inputs, number of nodes in each layer and the number

of outputs are not necessarily the same. For example, an ANN can consist of four inputs, five nodes in first hidden layer, eight nodes in second hidden layer, and one output.

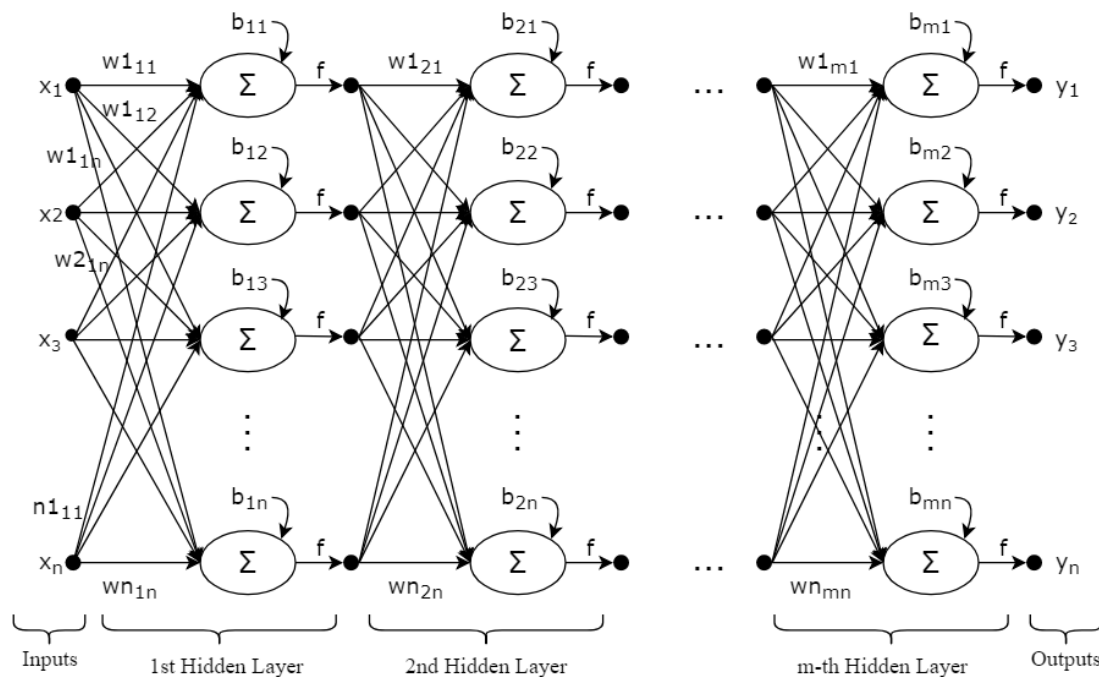
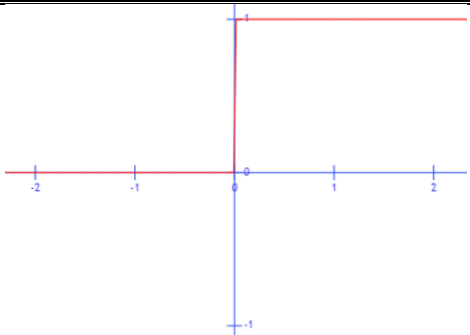
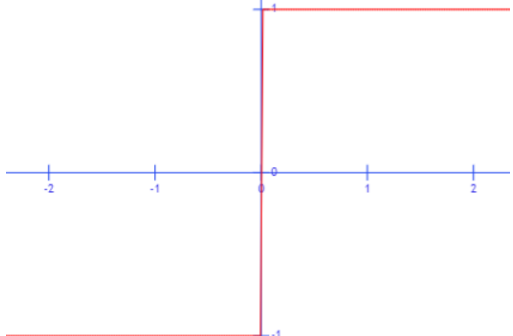
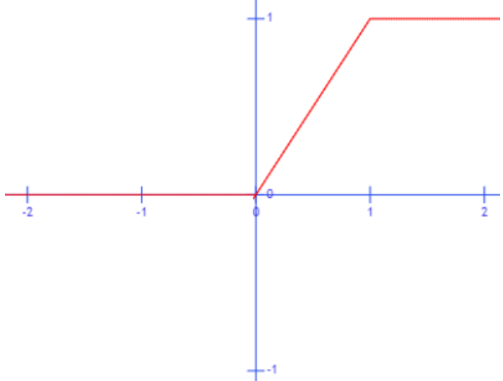


Figure 3- 13: ANN with m hidden layers and n nodes in each layer

3.3.2.3 Activation Functions

After integration of all the weighted inputs and bias for a single neuron, the value must go through an activation function to represent the output of the neuron. There are different activation functions suitable for different sorts of input and output data and which have to be selected based on the nature of the problem. Typical activation functions used in ANN are shown in Table 3- 1. Functions such as step function are good for sorting the input to categories for the output and functions like Hyperbolic Tangent and Sigmoid are suitable for nonlinear relationships between input and output data while a function like Ramp function is more suitable for linear approximation of data.

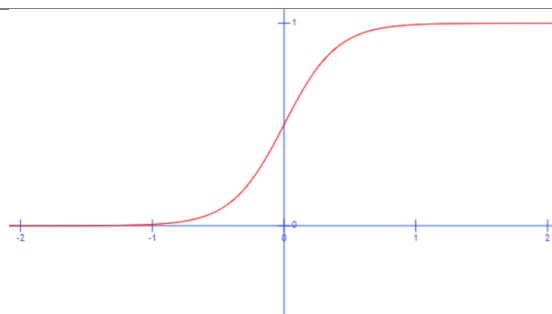
Table 3- 1: Typical activation functions used in ANNs

Name	Expression	Plot
Step Function	$y = \begin{cases} 1 & x \geq 0 \\ 0 & x < 0 \end{cases}$	
Hard Limit Function	$y = \begin{cases} 1 & x \geq 0 \\ -1 & x < 0 \end{cases}$	
Ramp Function	$y = \begin{cases} 1 & x > 1 \\ x & 0 \leq x \leq 1 \\ 0 & x < 0 \end{cases}$	

**Unipolar
Sigmoid
Function**

$$y = \frac{1}{1 + e^{-ax}}$$

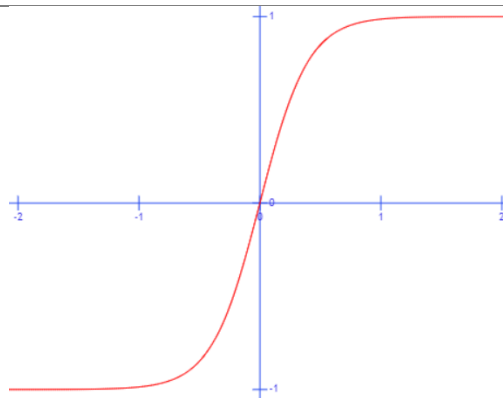
(plot for a=5)



**Bipolar
Sigmoid
Function**

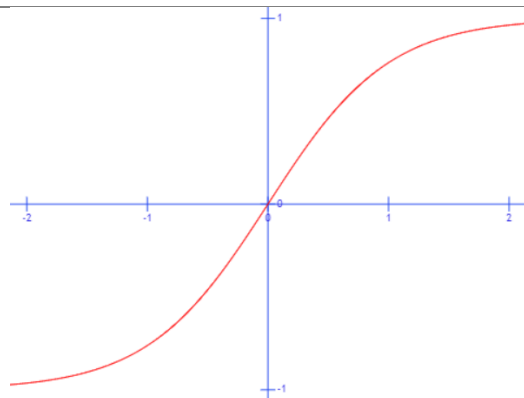
$$y = \frac{2}{1 + e^{-ax}} - 1$$

(plot for a=5)



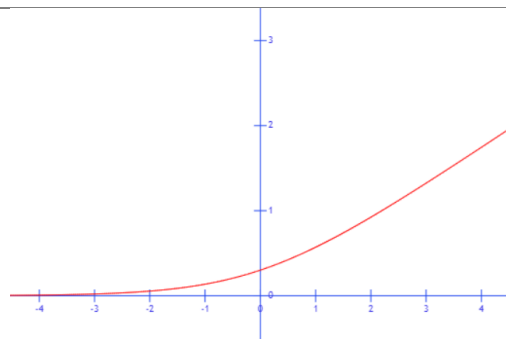
Tanh Function

$$y = \tanh(h)$$



Softplus

$$y = \log(1 + e^x)$$



3.3.2.4 Training Process

To train a neuron and the whole network in general means to adjust the values of weights and biases in order to get the most accurate output. There are two main methods for training a neural network: “supervised” method in which after each calculation the output of the network is compared with the output that is expected from the network and the weights and biases are adjusted based on how close these values are. This method is called “backpropagation” and was first proposed by Werbose (1974) and consists of using a minimization method such as steepest gradient method to minimize the difference between the calculated output and the existing output. This error calculation is also done on the level of each neuron and high errors relating to specific nodes will cause the weights of those nodes to be reduced so that their contribution to the overall output becomes less, resulting in a more accurate output. If the difference between the calculated output and expected values are less than the error tolerance, the networks is considered as trained and can be used to predict unknown values based on different inputs. On the other hand, “unsupervised” method automatically analyses the characteristics of the input and output data and determines which patterns and weights to use. In this study, supervised learning method is used. Another categorization of ANN training paradigms is fixed and adaptive training. In fixed training the number of nodes are fixed throughout the training however in adaptive method training starts with a relatively small number of nodes and if a threshold of iterations (epochs) is met, more nodes are added to the network. The later method can be useful for saving computational time as we all in cases which contain noise and more complex relation between the data.

There are two types of processing the output of the neurons: feedforward and feedback. In the feedforward method, the output of the neuron is never used again as its input and the flow of data is straight forward through the network whereas in feedback networks, the output of the neuron can be fed back into itself as a new input as shown in Figure 3-14.

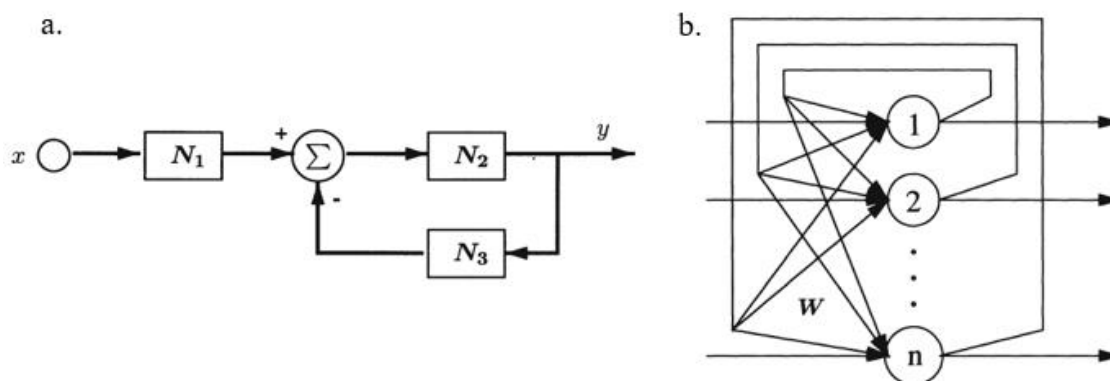


Figure 3- 14: a. single feedback neuron, b. simple feedback neural network (after Zhang (2000))

3.3.3 Developing an ANN for Nonlinear Material Behavior

To accurately predict nonlinear material behavior in nanoindentation tests a suitable number of layers and nodes in the proposed ANN shall be chosen. In the past years many researchers have used different ANN structures to predict nonlinear behavior of material which mostly consist of three or four layer ANNs. While selecting the input and output parameters for the ANN depends on the nature of the problem and type of behavior, the number of hidden layers usually does not exceed two, since too using a large number of hidden layers or too many nodes in each layer can cause divergence problems as well as

biased outputs toward the training data which means the trained model will have difficulty predicting material behavior using new input data. As a result, a neural network consisting of an input layer, two hidden layers and an output layer with adaptive learning was chosen for this study. The adaptive structure of the ANN was initially proposed by Ash (1989) called “Dynamic Node Creation Scheme” and further developed by Wu and Ghaboussi (1992) and further modified and used by Ghaboussi and Joghataie (1995), Ghaboussi et al. (1998), Muliana et al. (2002), and Haj Ali et al. (2008) and it was chosen for this study as well. However, the Dynamic Node Creation Scheme proposed by Ash (1989) consists a three-layer Neural Network that starts with a single node in the hidden layer and the algorithm continuously adds more nodes to the hidden layer until the convergence criteria is met. The decision that a new node needs to be added is made based on the gradient of slope of the average squared error (called “trigger slope”) in relation to the number of iterations (epochs) that have passed since the previous node was added. However, Wu and Ghaboussi (1992) mention that the selection of the “trigger slope” is highly dependent on the nature of the problem and the correct tolerance selection can greatly affect the convergence of the model. Thus, a fixed criteria in form of the maximum iterations after adding of each node was used in addition to the “trigger slope” method. After reaching the criteria for adding a new node to each of the hidden layers, the weights and biases of the existing connections are kept constant while the weights and biases of the new connections added with the new nodes are trained with a limited number of epochs. After that the constraint of the existing weights and biases is lifted and the training of the network is then resumed with the newly added and adjusted weights. The training then stops eventually when the convergence criteria, i.e. total error

becomes less than the error tolerance or the maximum number of epochs is reached, is reached and all the weights and biases of the trained network are stored as trained model parameters. The trained model is then used with other inputs that were not used in the training process and the outputs of the trained model are compared with the expected outputs to ensure the accuracy of the model.

To build the ANN for this study, an in-house code was developed using Python programming language which is very suitable for Machine Learning applications. The four-layer ANN was built in an object-oriented paradigm to ensure future readability and leave room for further adjustments such as adding the number of layers or manipulating the architecture of the neural network. The algorithm was adopted from Haj Ali et al. (2008) to implement the adaptive architecture for the ANN.

1. The available data is normalized to have values between 0 and 1 (or -1 and 1 depending on the nature of the problem and the type of activation functions used).
2. A percentage of available data, say 70% is selected as training data.
3. The initial number of nodes in the hidden layers is determined.
4. All the variables, i.e. weights and biases, are initialized using random values between 0 and 1.
5. Training is started by adjust the weights and biases to minimize the total error defined as: $E_{total} = \frac{1}{2} \sum (\mathbf{T} - \mathbf{O})^2$ (\mathbf{T} : Target values array, \mathbf{O} : Output values array)

I. Forward Propagation:

The inputs of the first hidden layer are the input values of the data set.

The inputs of the second hidden layer are the outputs of the first hidden layer and the inputs of the output layer are the outputs of the second hidden layer:

$$a_i = f(\sum w_j o_j + b_i)$$

where f is the activation function, w_j is the weight of each connection, b_i is the bias of each neuron, and a_i will eventually be the input for the next layer.

II. Backward Propagation:

Steepest gradient descent method is used to adjust the weights by calculating the needed change in the weight of each connection using the gradient of the error with respect to the connection weight:

$$\Delta w = \theta \frac{\partial E(w)}{\partial w}$$

in which θ is the learning rate. Assuming that the sigmoid function is used as activation function, we have:

$$f(x) = \frac{1}{1 + e^{-x}} \quad \text{and} \quad f'(x) = f(x)(1 - f(x))$$

Thus, for neurons that yield the final output layer, total error gradient with respect to the weights is calculated as:

$$\frac{\partial E(w_j)}{\partial w_j} = (t_j - o_j) f'(\sum w_j o_j) o_i$$

and for neurons that are in the hidden layers (note that node i is before j in layers):

$$\frac{\partial E(w_j)}{\partial w_j} = \sum \left(w_i \frac{\partial E(w_i)}{\partial w_i} \right) f'(\sum w_j o_j) o_i$$

Therefore, all weights are adjusted by their corresponding value of Δw .

6. If the gradient of the total error with respect to the number of iterations passed after the last node was added is less than the specified criteria or a certain number of epochs has passed, a new node is added:

All existing connection weights are stored and fixed. New connection weights and biases related to the new nodes are initialized. The new weights are then trained with a few iterations while the old weights are kept constant. After that all the fixes are released and training of the network is resumed by going back to step 5.

7. If the maximum number of total epochs has reached or the total error is less than the tolerance, the training is stopped and the values of weights and biases are stored as trained model parameters.
8. The rest of the data used in step 2 is used as prediction accuracy measurement.

3.3.4 Performance of the Developed ANN Model

The performance of the developed ANN model was studied by means of verification with available literature as well as convergence study to understand the limits and optimum architecture of the network. To verify the model, two nonlinear phenomena in literature were modeled. Nonlinear structural response data from a 25-element truss used by Ghaboussi et al. (1998) shown in Figure 3- 15 to train their ANN model and later used by Kim (2008) for verification of the ANN he proposed, was used as training and

verification data. An ANN with two hidden layers were used with different nodes in each layer to verify the performance of the developed ANN as well as observe the effect of number of nodes on nonlinear results. The structure of network was chosen similar to the one proposed in Kim (2008) so that the results of the studies are comparable. The first model had three nodes in each hidden layer with an error tolerance of 10% and the second model consisted of 15 nodes in each hidden layer with an error tolerance of 0.1%. As it can be seen in Figure 3- 16, the developed ANN model with the same structure as the one in Kim (2008) has better performance related to the number of epochs as well as the shape of the curve. For the models with 15 node, the difference is not significant but the number of epochs are again less that the ones in Kim (2008).

To investigate the effect of different number of nodes and hidden layers, the training data was chosen to be a nanoindentation load-displacement curve proposed by Kermouche et al. (2008). Performance of the developed ANN with two hidden layers was analyzed by varying the number of nodes in each hidden layer and using the nanoindentation curve as input and test data. As it can be seen in Figure 3- 17, a low number of nodes does not yield acceptable results but as the number of nodes increase, the error tolerance decreases and the shape of the curve becomes closer to the one using for the training. It should be noted that too many nodes in each layer will cause the model to over-fit the curve thus diverging from the actual results, therefore the optimum number of nodes in this case was approximately 16 for each of the two hidden layers.

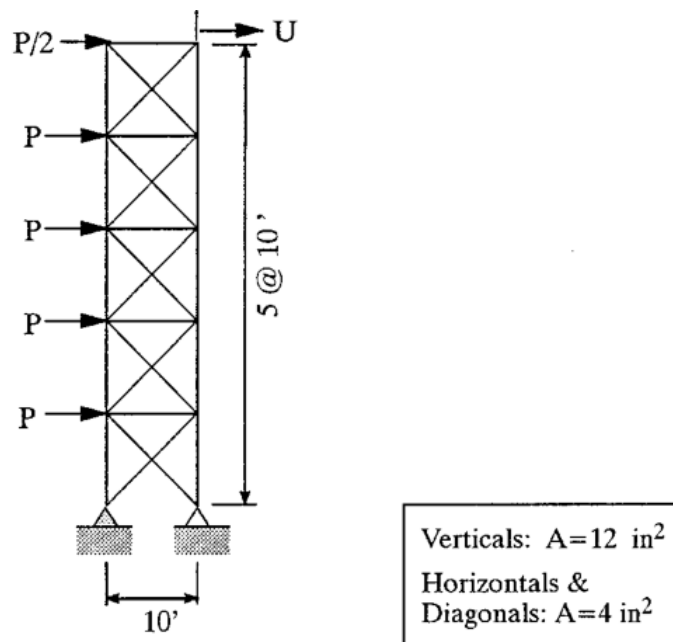


Figure 3- 15: The truss used by Ghaboussi et al. (1998) to verify their ANN model

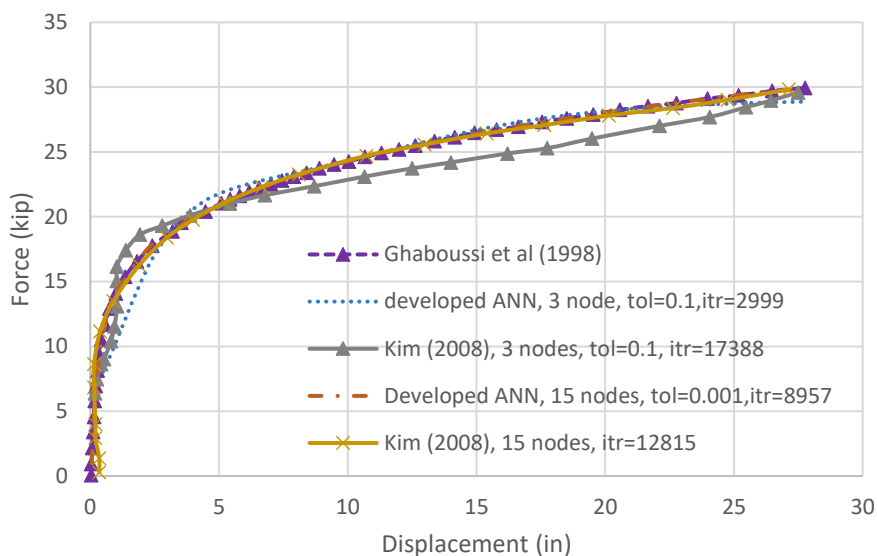


Figure 3- 16: Developed ANN model performance in comparison with the same model architecture proposed by Kim (2008)

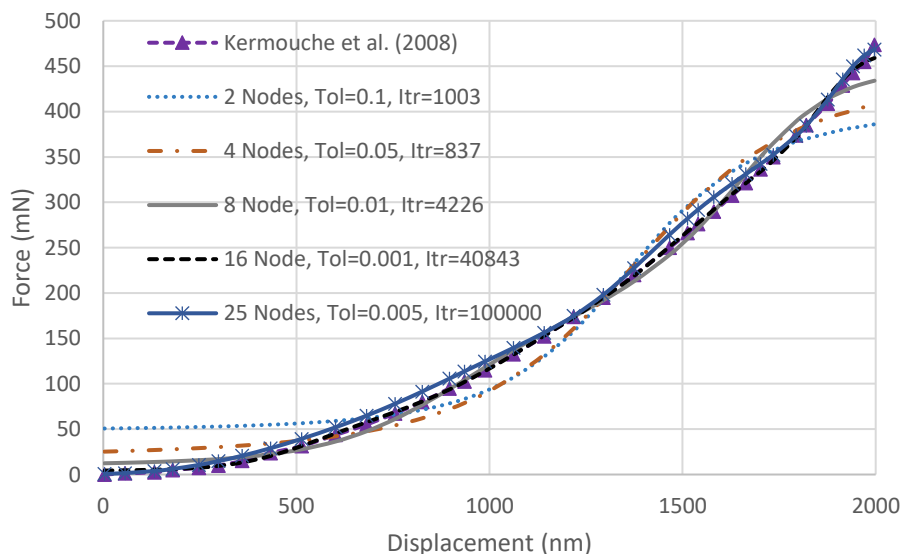


Figure 3- 17: Performance of developed 4-layer ANN in predicting nanoindentation results

3.3.5 Implementing the Nanoindentation Unloading Section in ANN

One of the major shortcomings of previous studies on nanoindentation tests with ANN is that most of the studies only take into account only the loading section of the curves (i.e. in Figure 3- 17). The reason for this problem is that if both loading and unloading parts

are used in the training of ANN, the ANN will not be able to distinguish between the loading and unloading sections due to the fact that a unique value for displacement will correspond to two values of load, one for loading and the other for unloading. This will cause losing the data of the unloading section which is an important part for understanding the plastic behavior of material in nanoindentation tests. As mentioned in Chapter 2, Tho et al. (2004) in addition to using load-displacement curves, used the area under the curves as input parameters to take into account the amount of plastic deformation in nanoindentation test. This approach however lacks the prediction of the shape of the unloading curve since it is difficult to find the exact shape of the unloading curve using the area under the curve. To overcome this problem, another approach was taken in the present study. To use both loading and unloading curves in the training data for ANN, a code was assigned to each part of the curve in the form of a 0 and 1. Therefore, in the dataset of the nanoindentation load-displacement points, a single point on the loading curve will be in the form of [displacement value, 0, force value] and a single point on the unloading curve will be in the form of [displacement value, 1, force value]. Adding the loading-unloading parameter to the data set might require more number of hidden layers in order for the ANN to be able to accurately predict the material behavior. In order to find the optimum number of hidden layers for this approach, a series of ANN training were performed while increasing the number of hidden layers, each with a constant number of nodes. However, the optimum number of hidden layers for this approach was found to be two. Figure 3- 18 and Figure 3- 19 show the effect of number of hidden layers on the performance of ANN for five and 10 nodes in each layer, respectively. It is worth noting that in case of 10 nodes in each layer, the two hidden layer

network showed better performance in achieving the error tolerance of 0.1% in a relatively low number of epochs whereas ANNs with higher number of hidden layers had difficulty converging the error tolerance and reached the cap for the number of epochs. Comparing the number of nodes in each layer for the 2-hidden layer network shows that the network with 10 nodes in each hidden layer yields better results.

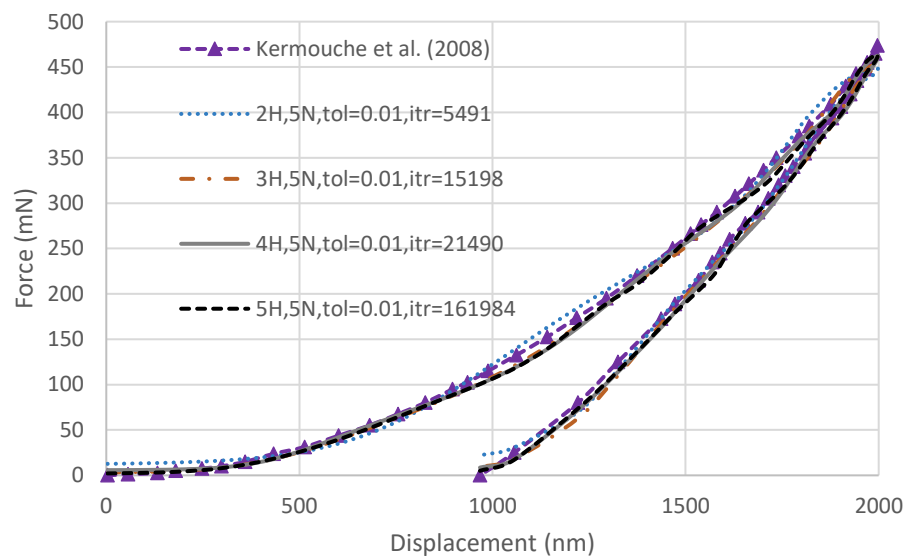


Figure 3- 18: Performance of ANN for predicting loading-unloading curve with different number of hidden layers with 5 nodes in each layer (H: number of hidden layers, N: Number of nodes)

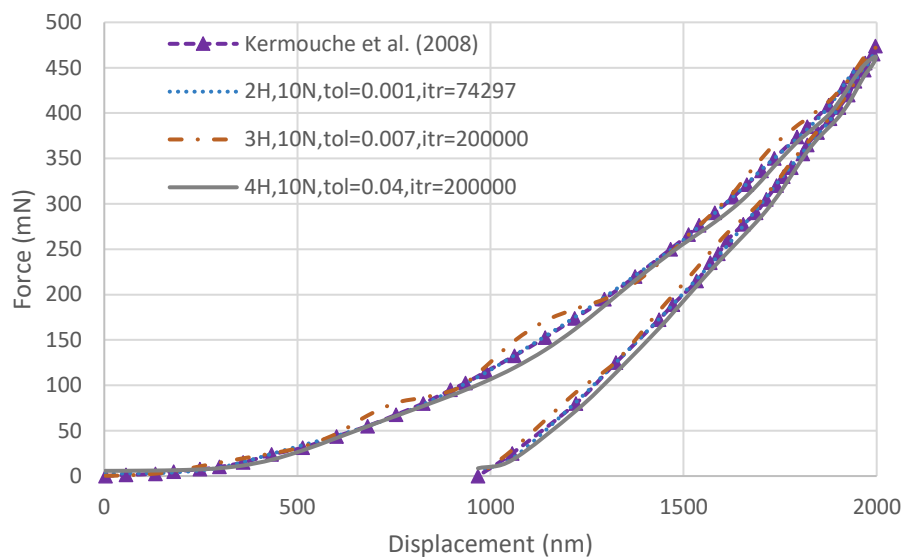


Figure 3- 19: Performance of ANN for predicting loading-unloading curve with different number of hidden layers with 10 nodes in each layer (H: number of hidden layers, N: Number of nodes) – Note: 5-hidden layer network did not converge

CHAPTER 4

RESULTS AND DISCUSSION

4.1 Nanoindentation Experiment Results

4.1.1 Fused Silica

Nanoindentation experiment were performed on the Fused Silica sample using conical and Berkovich indenter to investigate the effect of the indenter geometry on nanoindentation result as well as plastic behavior of this material in micro-scale. The results were plotted in a form of boundaries to avoid mixing up of many test result data and a mean was taken as a representative for comparison with test results as shown in Figure 4-1.

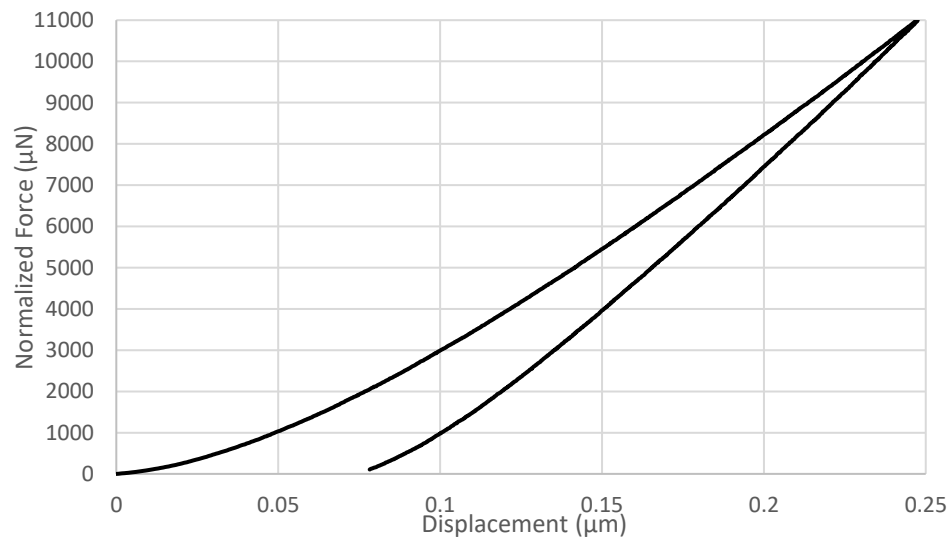


Figure 4- 1: Representative result of nanoindentation test on Fused Silica

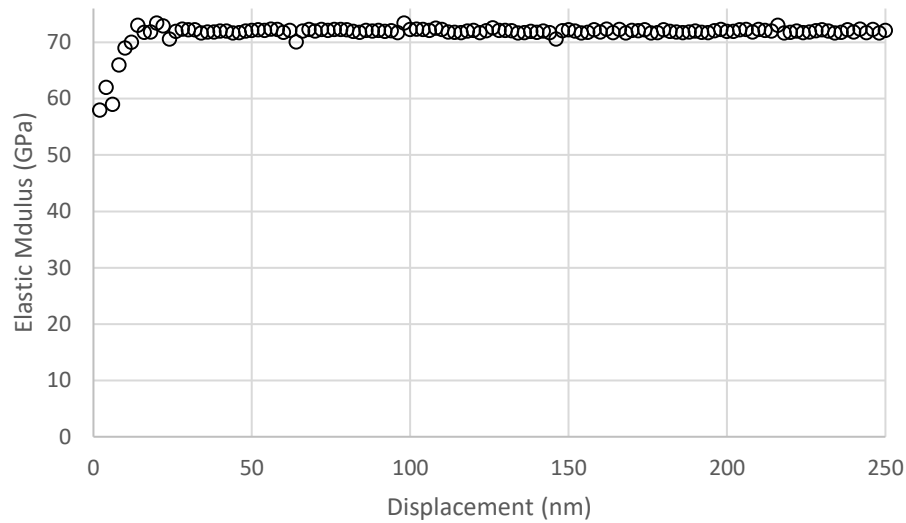


Figure 4- 2: Elastic modulus of Fused Silica for different indentation depths

4.1.2 Sand Grains

Previously polished samples as described in Chapter 3 were used in nanoindentation experiments to study the load-displacement curve as well as Young's modulus and hardness of sand grains. A representative load-displacement curve resulting in a Young's Modulus of 105 GPa was selected and is presented in Figure 4- 3, and the same curve was later used for comparison with FE simulation results. Although the results of nanoindentation tests were not as consistent as the results of the tests on Fused Silica, more than 70% of the tests resulted in a Young's modulus of approximately 105 GPa as shown in Figure 4- 4. Residual deformations on the sand grains that were represented in Figure 3- 5 is also illustrated in Figure 4- 5.

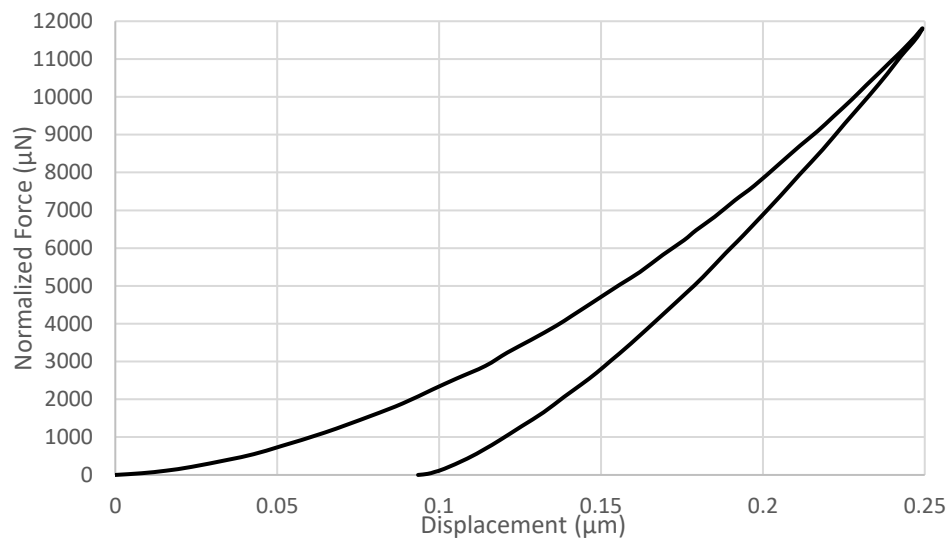


Figure 4- 3: Representative result of nanoindentation test on sand grains

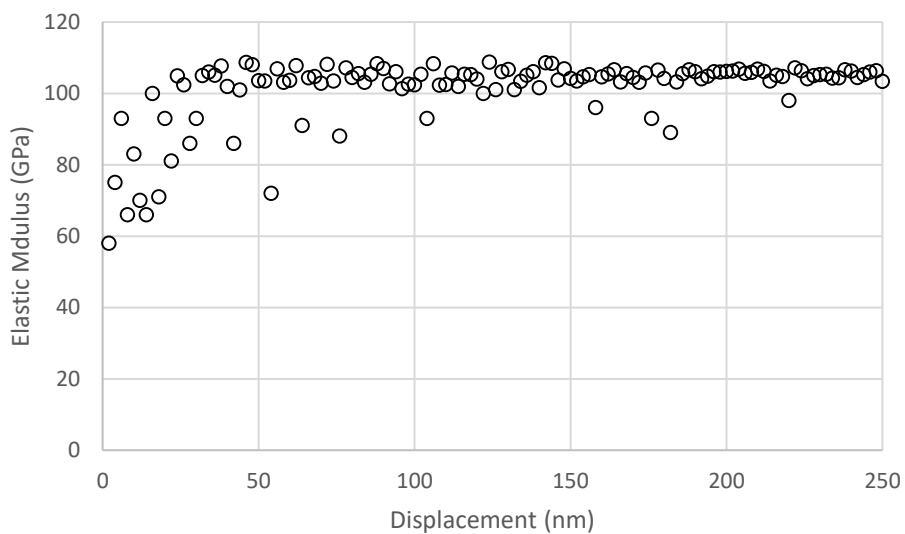
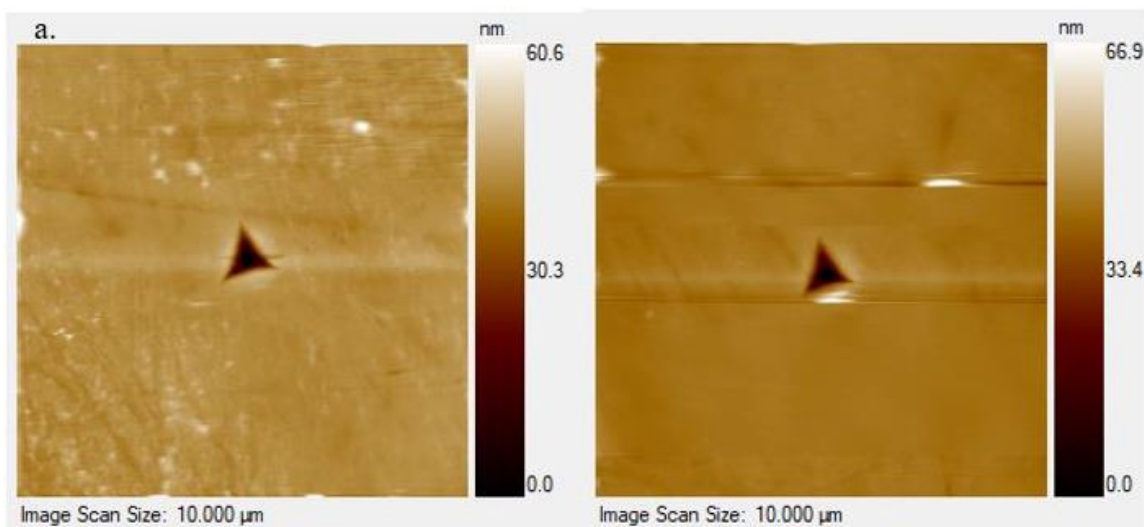


Figure 4- 4: Elastic modulus of sand grains for different indentation depths



b.

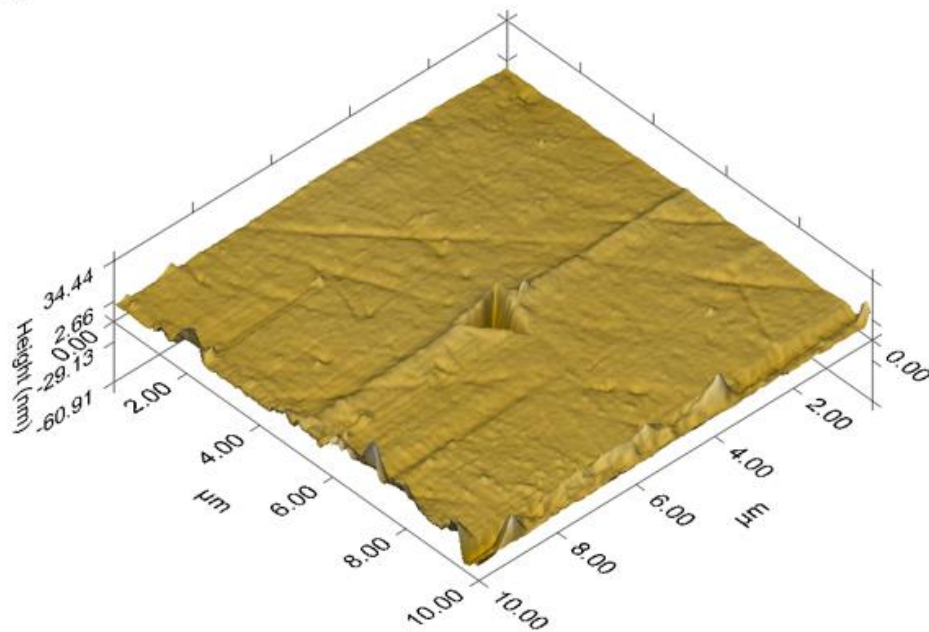


Figure 4- 5: Berkovich indenter residual imprint on sand grain

4.2 FEM Simulation Results

The first series of FE simulations were performed to investigate the effect of constitutive model used on the results in comparison with experimental data. An Elastic-Plastic (EP) yield criteria as well as the Modified Drucker-Prager/Cap (MDPC) model was used in the simulations. The starting values of the model parameters was chosen based on available literature which is shown in Table 4- 1. The FE results for a 45° conical indenter using the mentioned model parameter values were compared with nanoindentation experiment results as shown in Figure 4- 6.

FE simulation of nanoindentation tests on sand grains using Berkovich indenter was performed using the 2D equivalent 70.3° indenter using two different tip geometry. The sharp tip was modeled with a tip radius of 100 nm, the same value as the actual Berkovich indenter tip radius used in nanoindentation experiments and a blunt tip modeled as an indenter with tip radius of 1.4 μm. For these two tip geometries the two mentioned constitutive models were used with initial values shown in Table 4- 1. The results of FE simulation are compared with experimental data as illustrated in Figure 4- 7 and Figure 4- 8.

Comparing the results of simple Elastic-Plastic model with Modified Drucker-Prager/Cap model, it can be seen that for both cases of SiO₂, namely Fused Silica and sand grains, models yield better results when volumetric hardening is taken into account.

Table 4- 1: Initial model parameters* for FEM

Constitutive Model	Parameter	Value	
		Fused Silica**	Sand grain
Elastic-Plastic	Young's Modulus, E (GPa)	70.0	105.0
	Poisson's Ratio, ν	0.18	0.1
	Yield Stress, σ_y (GPa)	7.0	10.0
MDPC	Young's Modulus, E (GPa)	70.0	105.0
	Poisson's Ratio, ν	0.18	0.1
	Material Cohesion, d (GPa)	7.5	10.0
	Angle of Friction, β (°)	0.0001	0.0001
	Cap Eccentricity, R	1.53	1.0
	$\varepsilon_{vol}^{in} _0$	0	0
	α	1.0	1.0
MDCP Hardening Parameters	K	1.0	1.0
	Yield Stress (GPa) @ vol. strain=0	11.5	18.5
	Yield Stress (GPa) @ vol. strain=1%	12.5	19.5

* Refer to Section 3.2.1 for reference.

** Values from Bruns et al. (2017)

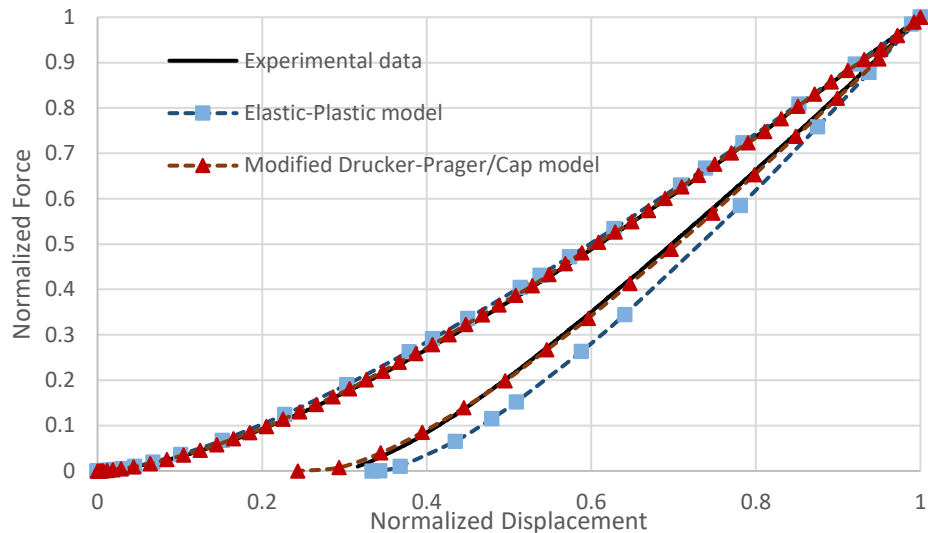


Figure 4- 6: FE simulation of Fused Silica with a conical indenter and two constitutive models

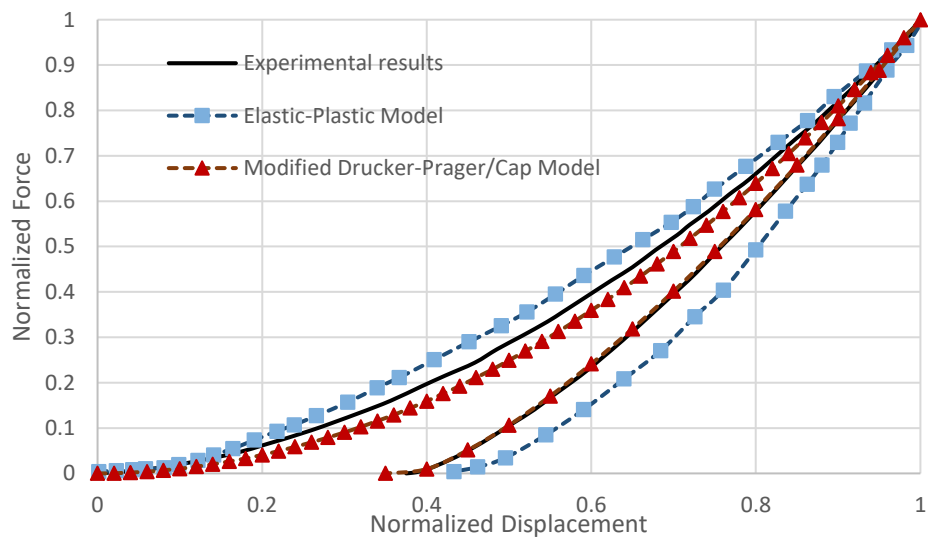


Figure 4- 7: FE simulation of sand grain with a sharp Berkovich equivalent indenter and two constitutive models

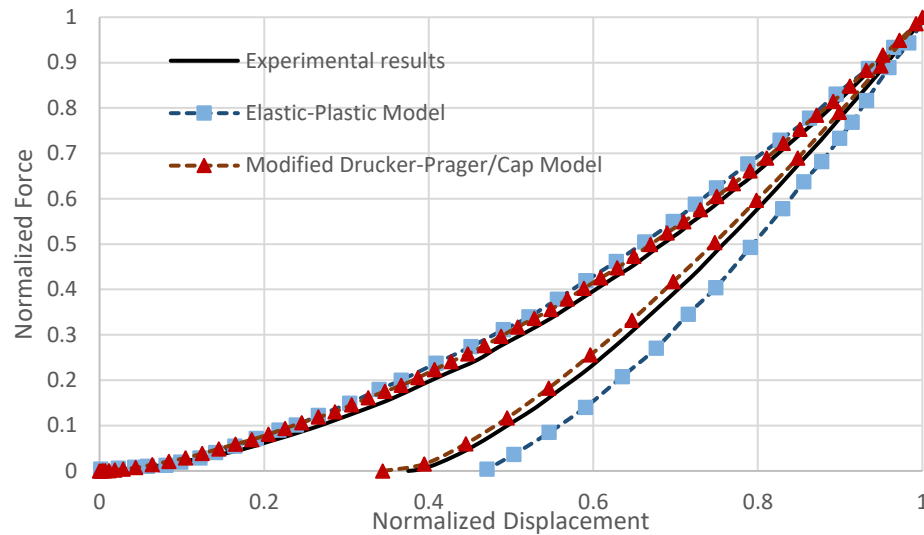


Figure 4- 8: FE simulation of sand grain with a blunt Berkovich equivalent indenter and two constitutive models

4.2.1 Effect of Indenter Tip Shape

Dependency of the FEM results on the tip geometry and shape including the face-to-centerline angle and tip radius was investigated and the results are shown in Figure 4- 9. It can be seen that a tip radius of 100 nm can have the same results as a sharp indenter and this is due to the amount of indenter surface in contact with the sample during indentation. For indentation depths higher than the tip radius, the tip bluntness will have little effect on the results and the face-to-centerline angle is the dominant geometry parameter in indentation test results. As for tip radius of 1.4 μm , since the indentation depth is smaller than the tip radius, the round shape of the tip affects the nanoindentation results.

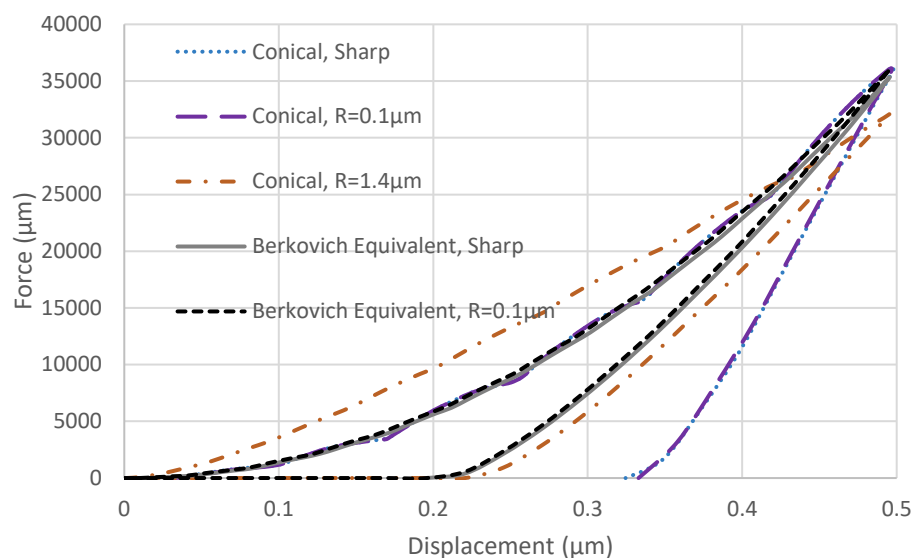


Figure 4- 9: FEM simulation of nanoindentation on Fuse Quartz using different indenter geometries

4.2.2 Plastic Deformations and Stresses

Investigating the shape of the deformed sample under maximum indentation depth as well as the residual deformation can provide a better understanding of the effect of indenter geometry as well as model parameters on nanoindentation test results. As it can be seen in Figure 4- 10, the stress values under maximum indentation depth as well as residual stress values are higher in case of the sharp conical indenter compared to the blunt conical indenter. The residual deformation also is different for two cases. Figure 4- 11 illustrates the same comparison for the Berkovich indenter and this comparison also shows higher stress values in both maximum depth and residual conditions for sharp Berkovich indenter. This difference is significantly less than the difference observed in case of the conical indenter because the bluntness of the Berkovich indenter refers to the tip radius of 100 nm whereas the bluntness in case of the conical indenter refers to the tip

radius of $1.4 \mu\text{m}$. Since the maximum depth is less than the tip radius in case of the Berkovich indenter, the indenter angle is the dominant shape parameter that affects the deformation as the same discussion made in previous section.

To investigate the effect of model plastic parameters in the shape of the residual deformation, a significantly lower material cohesion (i.e. parameter 'd' in Modified Drucker-Prager/Cap model in ABAQUS, $d=1.5 \text{ GPa}$) was chosen to compare the results with the original value of this parameter shown in Table 4- 1. Figure 4- 12 shows significantly higher amount of residual deformation and material pile-up compared to Figure 4- 10, and the same conditions can be observed in the load-displacement curves discussed in the next section.

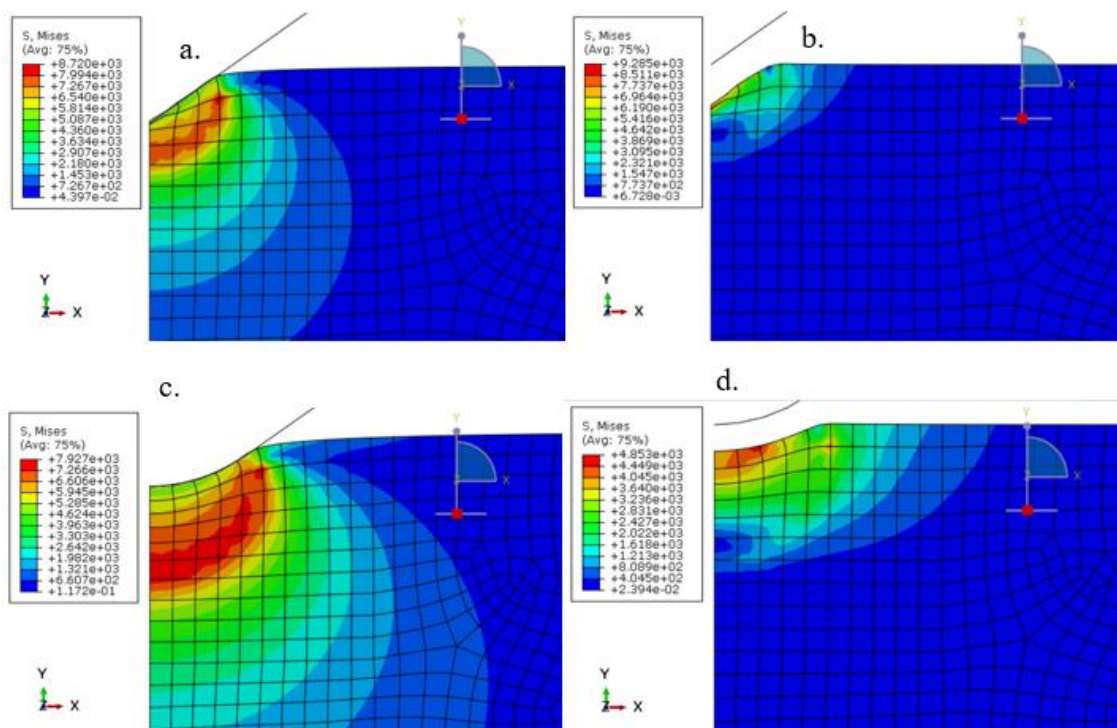


Figure 4- 10: Mises stress and sample deformation using: a. and b. sharp conical indenter, c. and d. blunt conical indenter (enlarged section of the model)

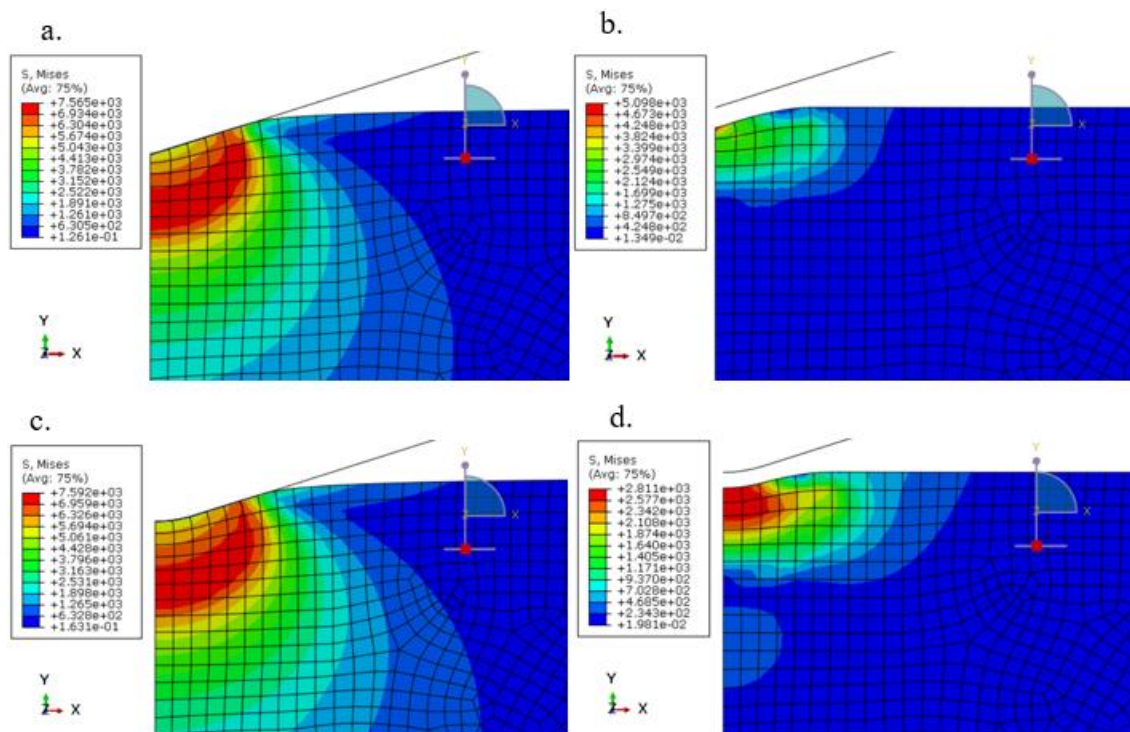


Figure 4- 11: Mises stress and sample deformation using: a. and b. sharp Berkovich indenter, c. and d. blunt Berkovich indenter (enlarged section of the model)

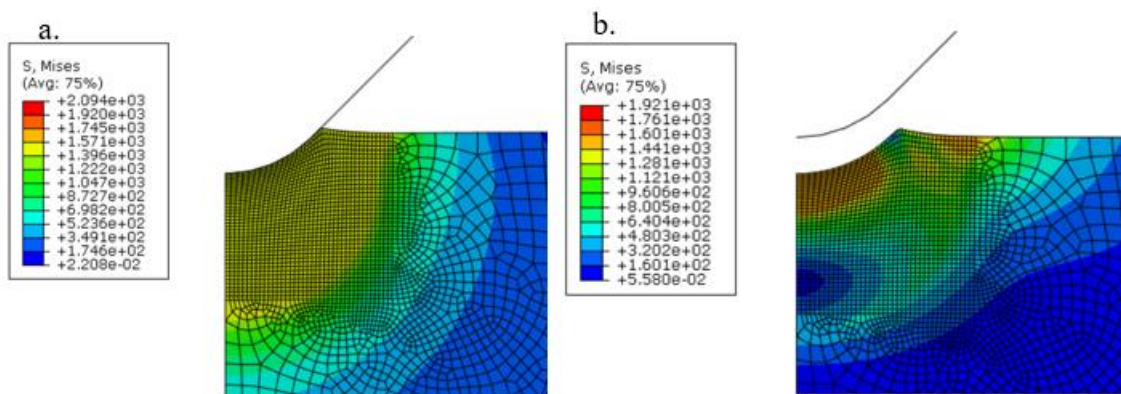


Figure 4- 12: Pile up and extreme residual deformation with low MDPC cohesion value (d=1.5 GPa) (enlarged section of the model)

4.2.3 Effect of Model Parameters

Sensitivity analysis of Modified Drucker-Prager/Cap model parameters were performed by changing the values of Elastic Modulus and material cohesion parameter (d) for the case of blunt conical indenter. It can be seen in Figure 4- 13 that for lower values of E , material does not enter the plastic region and the unloading curve is the same as the loading curve both with a low slope, whereas with increasing the value of E the slope increases and the unloading curve moves farther away from the loading curve and the residual plastic deformation increases as well. It is worth noting that the other parameter values were kept constant, having the values in Table 4- 1. To investigate the effect of material cohesion (i.e. parameter d) in MDPC model, the other parameters were kept constant and the value of d was increased as shown in Figure 4- 14. It can be seen that lower values of d causes the model to enter the plastic region faster and the reaction force has lower values in this case. Increasing the parameter d causes the reaction force to become higher therefore increasing the slope of the loading section of the curve. It can also be seen that the increase in value of d results in decrease of residual plastic deformation for the same maximum indentation depth. Changing the value of d in some cases caused interference with the cap parameters therefore they were changed accordingly while making sure it does not have any effects on the load-displacement curve.

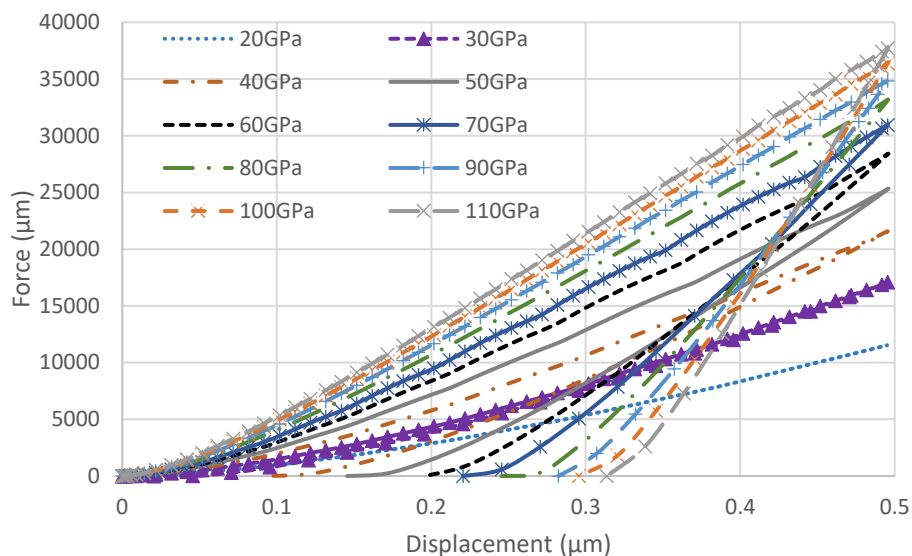


Figure 4- 13: Effect of Elastic modulus on load-displacement results of FE simulation using blunt conical indenter

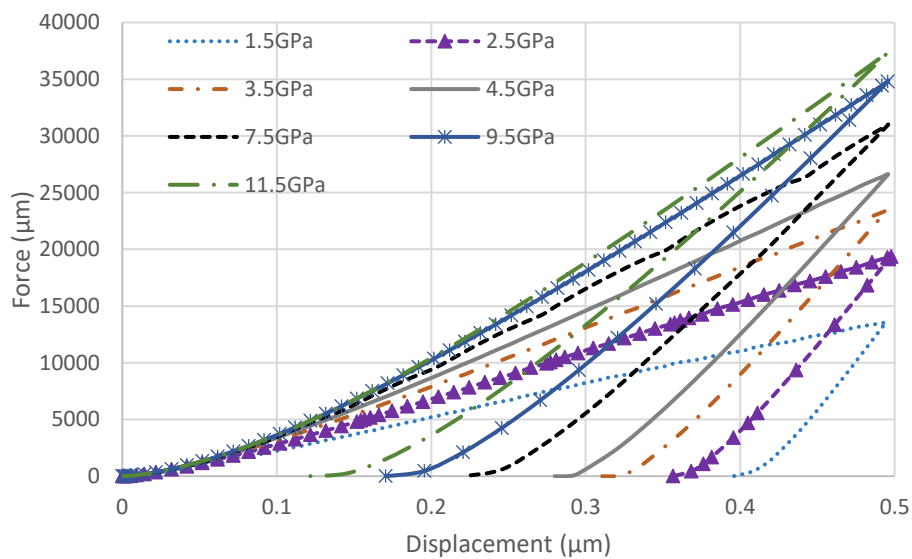


Figure 4- 14: Effect of material cohesion (d) on load-displacement results of FE simulation using blunt conical indenter

4.3 Artificial Neural Network Modeling Results

Input parameters of the ANN consisted of displacement, Elastic modulus and material cohesion and the output was load. The final trained model consisted of 15 neurons in each of the two hidden layers. FE simulation results in the form of load-displacement curves obtained from sensitivity analysis discussed in previous section were used to train and test the ANN model. Since the unloading section of the curves interfered with each other it was not possible to implement the loading and unloading section of the curves in the input data, therefore only the loading segments were used to train and test the model. Six loading curves were used to train the ANN model and after reaching an error value of 1% with approximately 1 million epochs, the weights and biases of the model were saved and used to test the model with the remaining values of the available data. Figure 4- 15 shows the loading curves used in the training of the ANN model and the values reached after the training are compared with FE results. The trained model predictions of the load values are shown in Figure 4- 16. As it can be seen the model successfully predicted the load values with the input parameters being displacement and Elastic modulus. The same approach was used to train and test the ANN for different values of material cohesion discussed in previous section, and the results of the training and testing of the ANN are shown in Figure 4- 17 and Figure 4- 18, respectively.

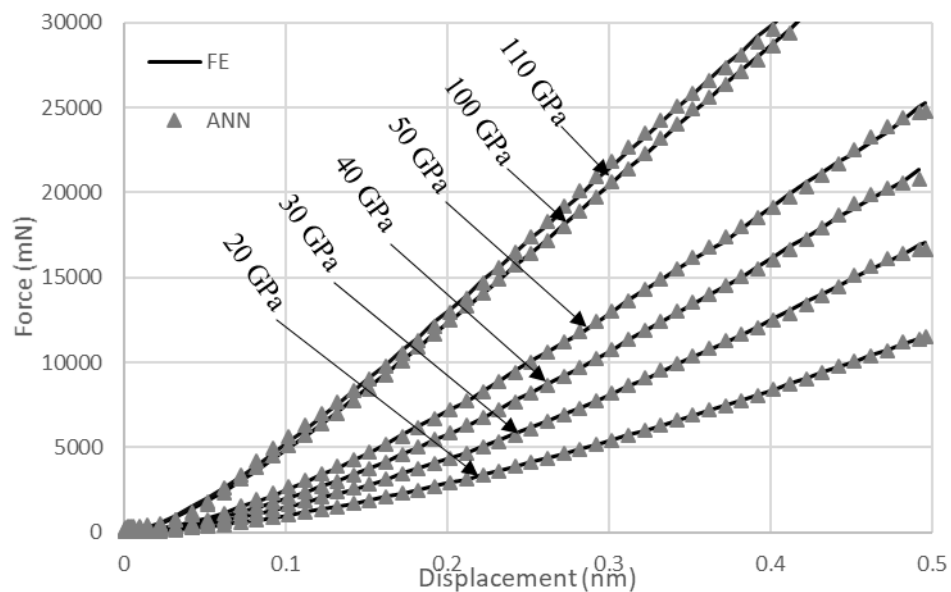


Figure 4- 15: Loading curves of different values of Elastic modulus used in ANN training

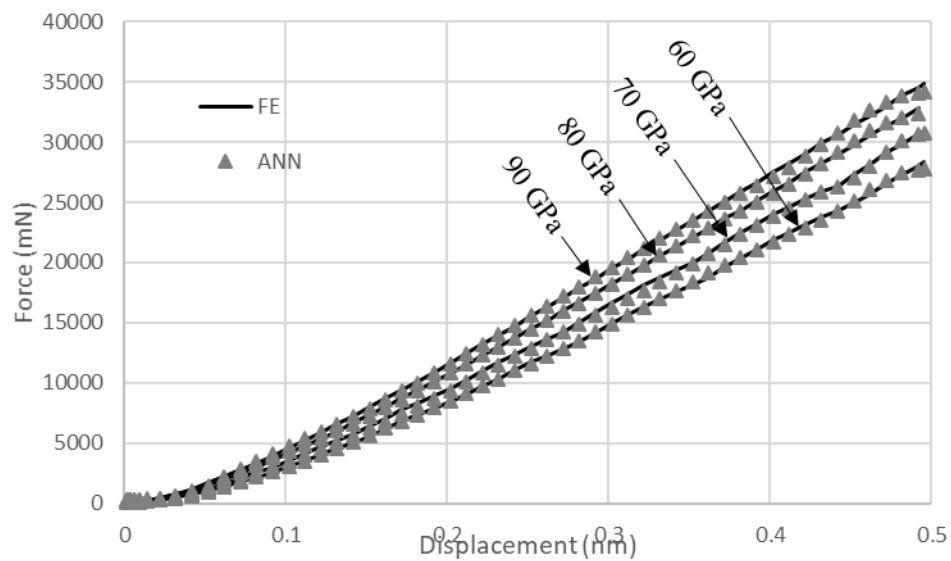


Figure 4- 16: ANN model prediction of loading curves of different values of Elastic modulus compared with FE results

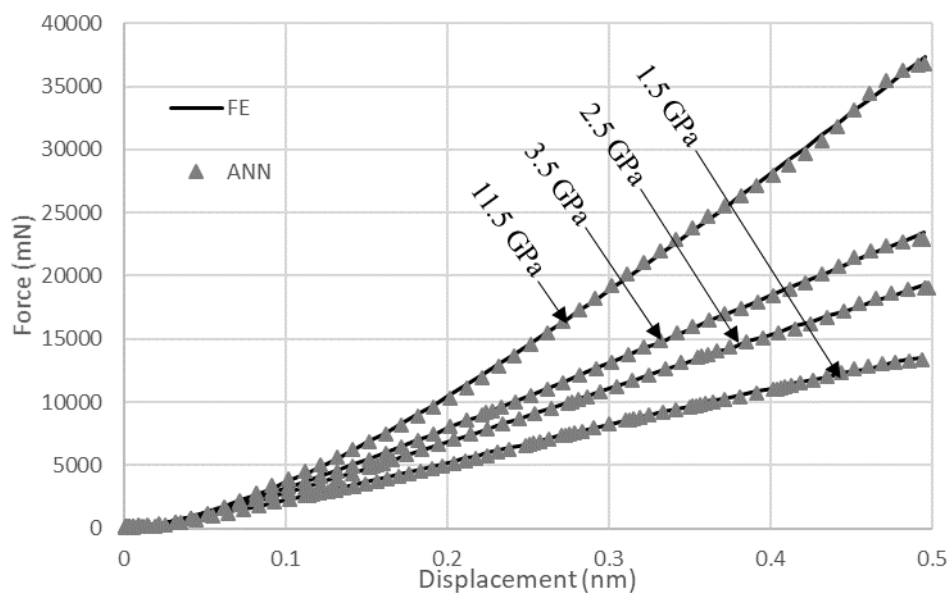


Figure 4- 17: Loading curves of different values of material cohesion used in ANN training

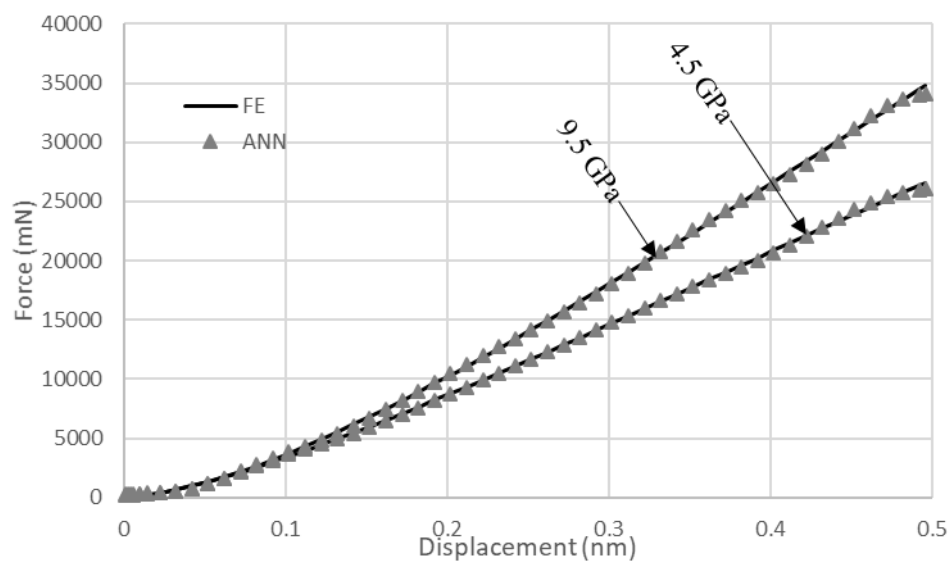


Figure 4- 18: ANN model prediction of loading curves of different values of material cohesion compared with FE results

If the ANN model is trained properly and with sufficient amount of data, it can then be used to predict the material behavior as discussed above. Figure 4- 19 shows the load-

displacement curves of nanoindentation using conical indenter for different values of Elastic modulus. FE simulations for these values were not performed but the trend and the limits and behavior of the curves seem to follow the same pattern and trend observed from FE simulations.

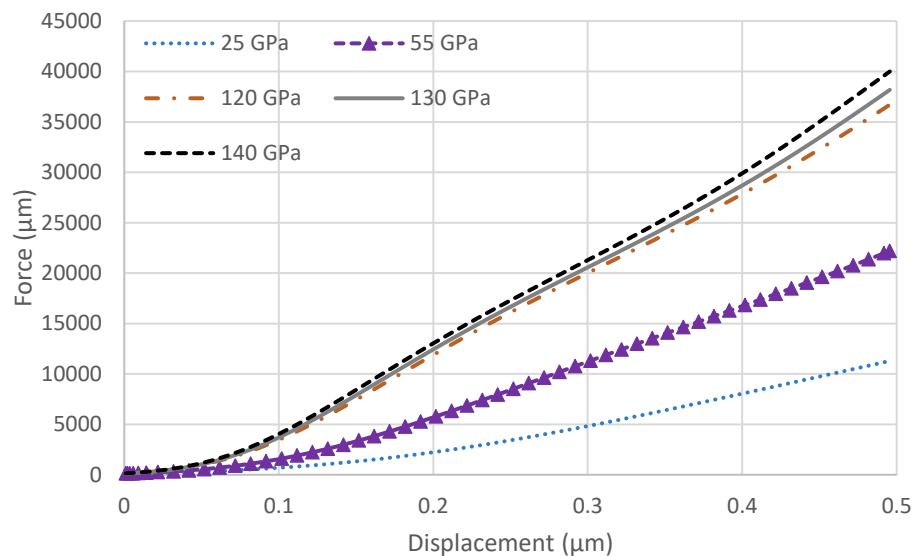


Figure 4- 19: Predicted load-displacement curves with different values of Elastic modulus

CHAPTER 5

CONCLUSION AND RECOMMENDATION

5.1 Summary and conclusion

In the present thesis, behavior of fused silica and individual sand grains under nanoindentation testing was investigated with an experimental approach followed by numerical Finite Element simulations and Artificial Neural Network Modeling. It was seen that despite brittle behavior of Fused Silica in macro-scale, plastic deformation can occur during nanoindentation tests, as well as volumetric hardening due to densification of material under the indenter tip. Nanoindentation tests on Fused Silica and sand grains showed that individual sand grains can have higher values of Elastic modulus and less residual plastic deformation compared to fused silica, however localized densification phenomenon was also the case for natural SiO_2 (i.e. sand grains). To model the material behavior, two constitutive models, i.e. Elastic-Plastic and Modified Drucker-Prager/Cap (MDPC) model were used in FE simulations and the accuracy of these models in predicting experimental test results were compared. It was observed that the MDPC model had a better accuracy provided that the model parameters are chosen accordingly. In both cases of Fused Silica and sand grains, using MDPC model to take into account the densification-induced volumetric hardening yielded significantly more realistic results compared to the simple Elastic-Plastic model. The effect of the model parameters on the final load-displacement curves of the nanoindentation simulations was analyzed by changing MDPC model parameters and performing FE simulations. The results were used for better understanding of the constitutive model as well as the micro scale

behavior of material. The influence of indenter tip geometry was investigated by modeling the 2D equivalent of a conical and a Berkovich indenter. It was observed that the tip radius and the face-to-centerline angle of the indenter can have a significant effect on the results. ANN models with different number of hidden layers and neurons were developed using Python programming language. The effect of different number of layers and neurons in the ANN model was investigated and a two-hidden-layer model was chosen for predicting nanoindentation test loading curve, since this model architecture showed better results in regard to the convergence and efficiency in predicting the results. The proposed ANN model was used along with FE simulation results to be trained to predict the FE simulation results for different constitutive model parameters. It was concluded that a well-trained ANN model can be a useful tool for predicting material response under nanoindentation loading.

5.2 Recommendation and Future Work

- Molecular Dynamics simulations can be a useful tool to further narrow down the scale of the study to molecular level. These simulations will provide a better understanding of the atomistic origins of plastic behavior of fused silica and sand grains. Dislocation of atoms under micro-scale loads is the main cause of densification behavior of this material and it can be further studied using MD simulations.
- High magnification and SEM imaging of the indenters used in nanoindentation tests can provide a better understanding of the geometry of the indenter as well as the difference between the nominal and actual tip radius. The tip of the indenter

usually becomes blunt with time and it can be useful to see the actual geometry of the indenter and simulate the exact shape in FEM models.

- Despite being computationally expensive, using 3D FEM simulations along with 2D simulations can ensure more realistic results especially in the case of Berkovich indenter since in the 2D studies only use an equivalent shape for this indenter.
- Developing other constitutive models that might be able to better capture the material behavior both in micro and macro scale can have a big impact of the scope of the material behavior in different scales.
- Using a more robust ANN and more computational power can include more complicated data for training and predicting the nanoindentation test results.

REFERENCES

- Oliver, W. C., & Pharr, G. M. (1992). An improved technique for determining hardness and elastic modulus using load and displacement sensing indentation experiments. *Journal of materials research*, 7(6), 1564-1583.
- Al-Rub, R. K. A., & Voyiadjis, G. Z. (2004). Analytical and experimental determination of the material intrinsic length scale of strain gradient plasticity theory from micro-and nano-indentation experiments. *International Journal of Plasticity*, 20(6), 1139-1182.
- Daphalapurkar, N. P., Wang, F., Fu, B., Lu, H., & Komanduri, R. (2011). Determination of mechanical properties of sand grains by nanoindentation. *Experimental Mechanics*, 51(5), 719-728.
- Dutta, A. K., & Penumadu, D. (2007). Hardness and modulus of individual sand particles using nanoindentation. In *Advances in Measurement and Modeling of Soil Behavior* (pp. 1-10).
- Wang, F., Fu, B., Mirshams, R. A., Cooper, W., Komanduri, R., & Lu, H. (2011). Mechanical properties measurement of sand grains by nanoindentation. In *Time Dependent Constitutive Behavior and Fracture/Failure Processes, Volume 3* (pp. 121-130). Springer, New York, NY.
- Kermouche, G., Barthel, E., Vandembroucq, D., & Dubujet, P. (2008). Mechanical modelling of indentation-induced densification in amorphous silica. *Acta Materialia*, 56(13), 3222-3228.
- Bruns, S., Johanns, K. E., Rehman, H. U., Pharr, G. M., & Durst, K. (2017). Constitutive modeling of indentation cracking in fused silica. *Journal of the American Ceramic Society*, 100(5), 1928-1940.
- Xin, K., & Lambropoulos, J. C. (2000, October). Densification of fused silica: effects on nanoindentation. In *Inorganic Optical Materials II* (Vol. 4102, pp. 112-122). International Society for Optics and Photonics.
- Torres-Torres, D., Muñoz-Saldaña, J., Gutierrez-Ladron-de Guevara, L. A., Hurtado-Macías, A., & Swain, M. V. (2010). Geometry and bluntness tip effects

on elastic–plastic behaviour during nanoindentation of fused silica: experimental and FE simulation. *Modelling and Simulation in Materials Science and Engineering*, 18(7), 075006.

- Marsh, D. (1964). Plastic flow in glass. *Proc. R. Soc. Lond. A*, 279(1378), 420-435.
- Lambropoulos, J. C., Xu, S., & Fang, T. (1996). Constitutive law for the densification of fused silica, with applications in polishing and microgrinding. *Journal of the American Ceramic Society*, 79(6), 1441-1452.
- Perriot, A., Vandembroucq, D., Barthel, E., Martinez, V., Grosvalet, L., Martinet, C., & Champagnon, B. (2006). Raman microspectroscopic characterization of amorphous silica plastic behavior. *Journal of the American Ceramic Society*, 89(2), 596-601.
- Moya, A., & Irikura, K. (2010). Inversion of a velocity model using artificial neural networks. *Computers & Geosciences*, 36(12), 1474-1483.
- Messikh, N., Bousba, S., & Bougdah, N. (2017). The use of a multilayer perceptron (MLP) for modelling the phenol removal by emulsion liquid membrane. *Journal of Environmental Chemical Engineering*, 5(4), 3483-3489.
- Park, Y. S., & Lek, S. (2016). Artificial Neural Networks: Multilayer Perceptron for Ecological Modeling. In *Developments in Environmental Modelling* (Vol. 28, pp. 123-140). Elsevier.
- Sidarta, D. E., & Ghaboussi, J. (1998). Constitutive modeling of geomaterials from non-uniform material tests. *Computers and Geotechnics*, 22(1), 53-71.
- Ghaboussi, J., & Sidarta, D. E. (1998). New nested adaptive neural networks (NANN) for constitutive modeling. *Computers and Geotechnics*, 22(1), 29-52.
- Fu, Q., Hashash, Y. M., Jung, S., & Ghaboussi, J. (2007). Integration of laboratory testing and constitutive modeling of soils. *Computers and Geotechnics*, 34(5), 330-345.
- Haj-Ali, R., Kim, H. K., Koh, S. W., Saxena, A., & Tummala, R. (2008). Nonlinear constitutive models from nanoindentation tests using artificial neural networks. *International Journal of Plasticity*, 24(3), 371-396.

- Muliana, A., Haj-Ali, R. M., Steward, R., & Saxena, A. (2002). Artificial neural network and finite element modeling of nanoindentation tests. *Metallurgical and Materials Transactions A*, 33(7), 1939-1947.
- Chamekh, A., Salah, H. B. H., & Hambli, R. (2009). Inverse technique identification of material parameters using finite element and neural network computation. *The International Journal of Advanced Manufacturing Technology*, 44(1-2), 173.
- Tyulyukovskiy, E., & Huber, N. (2006). Identification of viscoplastic material parameters from spherical indentation data: Part I. Neural networks. *Journal of materials research*, 21(3), 664-676.
- Tho, K. K., Swaddiwudhipong, S., Liu, Z. S., & Hua, J. (2004). Artificial neural network model for material characterization by indentation. *Modelling and Simulation in Materials Science and Engineering*, 12(5), 1055.
- Huber, N., Nix, W. D., & Gao, H. (2002, July). Identification of elastic-plastic material parameters from pyramidal indentation of thin films. In *Proceedings of the Royal Society of London A: Mathematical, Physical and Engineering Sciences* (Vol. 458, No. 2023, pp. 1593-1620). The Royal Society.
- Bulychev, S. I., Alekhin, V. P., Shorshorov, M. K., Ternovskij, A. P., & Shnyrev, G. D. (1975). Determination of Young modulus by the hardness indentation diagram. *Zavodskaya Laboratoriya*, 41(9), 1137-1140.
- Pharr, G. M., Oliver, W. C., & Brotzen, F. R. (1992). On the generality of the relationship among contact stiffness, contact area, and elastic modulus during indentation. *Journal of materials research*, 7(3), 613-617.
- Doerner, M. F., & Nix, W. D. (1986). A method for interpreting the data from depth-sensing indentation instruments. *Journal of Materials research*, 1(4), 601-609.
- SILICA, U. (2008). Product Data. *Pan*, 140(200), 270.
- Zhang, X. S. (2000). Feedback Neural Networks. In *Neural Networks in Optimization* (pp. 137-175). Springer, Boston, MA.

- Werbos, P. (1974). Beyond regression: new fools for prediction and analysis in the behavioral sciences. PhD thesis, Harvard University.
- McCulloch, W. S., & Pitts, W. (1943). A logical calculus of the ideas immanent in nervous activity. The bulletin of mathematical biophysics, 5(4), 115-133.
- Ghaboussi, J., & Joghataie, A. (1995). Active control of structures using neural networks. Journal of Engineering Mechanics, 121(4), 555-567.
- Wu, X., Ghaboussi, J., & Garrett Jr, J. H. (1992). Use of neural networks in detection of structural damage. Computers & structures, 42(4), 649-659.
- Ghaboussi, J., Pecknold, D. A., Zhang, M., & Haj-Ali, R. M. (1998). Autoprogressive training of neural network constitutive models. International Journal for Numerical Methods in Engineering, 42(1), 105-126.
- Ash, T. (1989). Dynamic node creation in backpropagation networks. Connection science, 1(4), 365-375.
- Kim, H. K. (2008). Multi-scale nonlinear constitutive models using artificial neural networks. Georgia Institute of Technology.
- Li, W., Rieser, J. M., Liu, A. J., Durian, D. J., & Li, J. (2015). Deformation-driven diffusion and plastic flow in amorphous granular pillars. Physical Review E, 91(6), 062212.
- Maloney, C. E., & Lemaître, A. (2006). Amorphous systems in athermal, quasistatic shear. Physical Review E, 74(1), 016118.
- Le Bouil, A., Amon, A., McNamara, S., & Crassous, J. (2014). Emergence of cooperativity in plasticity of soft glassy materials. Physical review letters, 112(24), 246001.